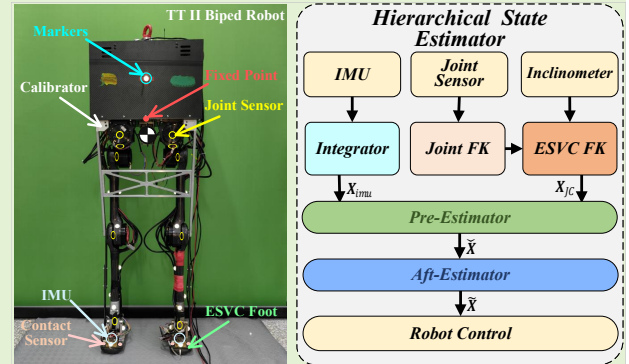


# Noise Analysis and Hierarchical Adaptive Body State Estimator For Biped Robot Walking With ESVC Foot

Boyang Chen, Xizhe Zang, Chao Song, Yue Zhang, Xuehe Zhang and Jie Zhao

**Abstract**—The ESVC(Ellipse-based Segmental Varying Curvature) foot, a robot foot design inspired by the rollover shape of the human foot, significantly enhances the energy efficiency of the robot walking gait. However, due to the tilt of the supporting leg, the error of the contact model are amplified, making robot state estimation more challenging. Therefore, this paper focuses on the noise analysis and state estimation for robot walking with the ESVC foot. First, through physical robot experiments, we investigate the effect of the ESVC foot on robot measurement noise and process noise. and a noise-time regression model using sliding window strategy is developed. Then, a hierarchical adaptive state estimator for biped robots with the ESVC foot is proposed. The state estimator consists of two stages: pre-estimation and post-estimation. In the pre-estimation stage, a data fusion-based estimation is employed to process the sensory data. During post-estimation, the acceleration of center of mass is first estimated, and then the noise covariance matrices are adjusted based on the regression model. Following that, an EKF(Extended Kalman Filter) based approach is applied to estimate the centroid state during robot walking. Physical experiments demonstrate that the proposed adaptive state estimator for biped robot walking with the ESVC foot not only provides higher precision than both EKF and Adaptive EKF, but also converges faster under varying noise conditions.

**Index Terms**— Adaptive state estimation, biped locomotion, curvature foot, noise measurement.



## I. INTRODUCTION

**B**IPEDAL robot technology has made significant progress in recent years, such as G1 from Unitree [1], Atlas of Boston Dynamics [2] and Digit designed by Agility Robotics [3]. In laboratory environment, robots have already demonstrated impressive motion capabilities that are close to, or even surpass, those of humans. However, from the prospective of practical application, numerous challenges still exist, among which gait energy efficiency and ground adaptability are particularly important. When excluding upper limb operations, the foot, as the only part interacting with the external environment, directly affect the evolution of the entire robot system. Therefore, to improve bipedal walking performance, various foot designs for different scenarios have been investigated and implemented [4] [5] [6] [7].

This work was supported in part by the Major Research Plan of the National Natural Science Foundation of China (92048301).

Boyang Chen, Xizhe Zang, Chao Song, Yue Zhang, Xuehe Zhang and Jie Zhao are with the School of Mechatronics Engineering, Harbin Institute of Technology, Harbing 150001, China (e-mail: chenboyang@stu.hit.edu.cn, zangxizhe@hit.edu.cn, songchao@stu.hit.edu.cn, yzhanghit@stu.hit.edu.cn, zhangxuehe@hit.edu.cn, jzhao@hit.edu.cn).

Corresponding authors: Xuehe Zhang.

Among these studies, a key question is that how to effectively integrate foot design with robot locomotion and fully exploit the performance enhancements provided by the meticulous foot designs. This question is challenging and a prerequisite is that how the foot designs influence locomotion dynamics. In particular, the impact of the foot designs on walking-state variations needs careful consideration. In other words, from a feedback control perspective, understanding the effect of foot design on system noise and ensuring accurate state estimation are indispensable.

In terms of rollover shape, mainstream robot foot designs can be categorized as: arched foot [8], point foot [9], flat foot [10], line foot [11], arc/curved foot [6] [12], bionic foot [13] and flexible heterogeneous foot [14]. Among them, point foot, line foot, and flat foot are the most widely used. The point foot, with negligible mass, maintains point contact with the ground at all times in both the sagittal and coronal planes, greatly simplifying the modeling and control of biped robots, but it cannot provide sufficient frictional torque. The line foot maintains line contact in the sagittal plane and point contact in the coronal plane, compensating for the lack of friction of point foot. However, its energy efficiency is much lower than that of arc/curved or bionic designs. Moreover, line foot

and point foot lack sufficient sensory equipment so the foot data and body state have to be estimated through additional methods. The flat foot can compensate for the shortcomings of both; however, maintaining full contact requires the supporting foot to remain parallel to the ground at all times. This necessitates actuation of the ankle joint in both the pitch and roll directions, which in turn hinders the mass centralization of the robot. Additionally, the impact energy dissipation caused by the contact also results in lower gait efficiency. The bionic foot and flexible heterogeneous foot are not discussed in this paper due to their complexity and specific application scenarios.

In fact, it is difficult to find a generalized principle for robot foot design currently, especially when balancing multiple design criteria. Therefore the rollover shape of human foot serves as a good bionic template. Researchers in prosthetics and human anatomy have found that the bionic rollover shape can be divided into three parts: the fore-foot, mid-foot, and hind-foot. Each segment exhibits a varying curvature, with the heel and toes being more curved, while the mid segment remains relatively flat. The segmented varying curvature configuration allows for higher energy efficiency during human biped walking [15] [16] [17]. Inspired by this an ellipse based segmental varying curvature foot (ESVC foot) has been proposed in our previous work [12]. Multiple elliptical arcs are engaged to approximate the configuration of the rollover shape of human foot. Physical experiments on TT II robot illustrate that the foot design significantly improves the gait energy efficiency, especially when there exists lateral velocity. During walking, the support leg of the robot with ESVC foot undergoes a passive rotation in coronal plane and the contact point will rollover along the elliptical arcs. As the analytical form of the contact model does not exist due to the incomplete elliptic integral, an approximation contact model based on elementary functions is provide in our previous research. However, despite the simplicity of this method, the modeling error cannot be eliminated, and the error is amplified by the support leg rotation during robot walking. This means that directly using joint state data to obtain the robot body state is too coarse and sensitive for feedback control. Hence, this paper we try to reveal how the ESVC foot affect noise distribution of the robot system and focuses on the state estimation with ESVC foot.

The state estimation of bipedal robot has long been a focus of researchers, as it serves as a crucial foundation for feedback control. Due to the high dimensional non-linearity of the legged robot system, the extended Kalman filter(EKF) based method is widely used for state estimation [18], [19], [20], [21], [22]. By setting the process noise and measurement noise covariance as constant, Chen et al. [19] used the EKF to estimate the state of a fixed point(FP). The center of mass(CoM) state is then approximated through the FP and incorporated into feedback control based on the linear inverted pendulum model. This method is suitable for slower robot walking, where the FP behaves similarly to the CoM. Kang et.al. [20] proposed a nonlinear distributed state estimation framework for legged robot system. Through EKF and moving horizon estimation, the linear and angular states of the robot floating base can be estimated decoupledly, while maintaining a balance between

accuracy and computational efficiency is feasible. Gao et al. [22] proposed a robust adaptive state estimator based on the Invariant Extended Kalman Filter(IEKF), and by segmenting the design of adaptive adjustment factors, the estimator can adjust the noise covariance dynamically, and in their physical experiments, the velocity estimation of CoM demonstrated around 50% improvement compared to the original IEKF. Kim et.al. [23] redefined the state estimation as a Maximum A Posteriori (MAP) problem, achieving estimation results comparable to the IEKF under different contact conditions. Youm et.al. [24] proposed a learning-based approach that combines the Neural Measurement Network with EKF, significantly reducing position drift. The network is trained using only simulation data.

This paper focuses on the impact of the ESVC foot to the system noise and state estimation of walking bipedal robots. The contributions are as follows: first, we investigate the impact of the ESVC foot and contact model error on the robot measurement noise and process noise through physical experiments. Then a temporal regression model for noise covariance is developed using sliding window strategy and weighted cubic regression. Finally, we propose a hierarchical adaptive state estimator based on the temporal model. Under feedback control using the Hybrid Linear Inverted Pendulum (HLIP) [25], the proposed state estimator not only accurately provides body state data during robot walking, but also converges rapidly when the walking gait varying, compared to the classical EKF and the adaptive variants with fixed noise covariance.

The organization of this paper is as follows: In Section II.a, we review the ESVC foot model and demonstrate how to obtain the sensory data of robot state through the approximation model. In Section II.b, we first reveal the distribution of measurement noise and process noise through fixed point trajectory tracking experiments and physical walking experiments, respectively. Then the temporal regression model is designed for the initial guess of estimation. In Section III, we discuss the hierarchical adaptive state estimator. Section IV presents the validation and evaluation of the proposed state estimator. Conclusions and future work are presented in Section V.

## II. NOISE ANALYSIS AND APPROXIMATION

### A. Sensory State Data Acquisition

The quality of sensory data directly impacts the body state estimation, especially when errors are introduced by the varying contact point model of the ESVC foot. In order to investigate the impact, we equipped the ESVC foot to bipedal robot TT II as shown in the abstract figure. To acquire the sensory body state data relative to the contact frame, including the center of mass and the swing foot, six virtual joints are typically introduced to describe the robot motion with respect to the inertial frame which allows the body state can be calculated in a manipulator-like manner. However, this method is susceptible to sensory noise and also increases the computational load on the onboard controller. In our previous work [12], we derived the spatial transformation matrices

of foot upper center frame, foot fixed frame and contact point frame. Through the ESVC kinematics, we divide the configuration space into the internal space and the external space and the robot body state can be computed efficiently and decoupledly within the two spaces. In the internal space, the robot can be regarded as being fixed to the ground at the upper center frame of the support foot, making the sensory body state data only dependent on the joint states:

$$\mathbf{X}^{O_i} = f(\mathbf{q}_i, \dot{\mathbf{q}}_i). \quad (1)$$

For simplicity, we use  $O_i$  and  $C$  to denote the upper center frame of the support foot and contact frame, respectively. Then, in the external space, the sensory body state from joint space data calculation  $\mathbf{X}_{JC} = [\mathbf{p}_{JC}^C, \mathbf{v}_{JC}^C]^T$  with respect to the inertial frame can be obtained through the matrix  ${}^C_{O_i}\mathbf{T}_E$  and its derivatives  ${}^C_{O_i}\dot{\mathbf{T}}_E$ , which represents the transformation between frame  $O_i$  and frame  $C$  of ESVC foot, as shown in Eq.2. Since the transformation matrix is based on elementary functions and the derivatives can be obtain directly through numerical differencing, the calculation of the external space is simplified to a single matrix multiplication:

$$[\mathbf{p}_{JC}^C, 1, \mathbf{v}_{JC}^C, 1]^T = \begin{bmatrix} {}^C_{O_i}\mathbf{T}_E & 0 \\ {}^C_{O_i}\dot{\mathbf{T}}_E & {}^C_{O_i}\mathbf{T}_E \end{bmatrix} [\mathbf{p}^{O_i}, 1, \mathbf{v}^{O_i}, 1]^T \quad (2)$$

TT II robot is equipped with three groups of IMU and inclinometers, as shown in the top-right subfigure of the abstract figure. As two sensor groups are mounted on the surface of the ESVC foot to directly provide the states of both the swing and support foot, the matrix  ${}^C_{O_i}\mathbf{T}_E$  and  ${}^C_{O_i}\dot{\mathbf{T}}_E$  in Eq.2 can be calculated accordingly. The third group is mounted at a fixed position(FP) which is close to the CoM when standing, to obtain approximate state data of the CoM  $\mathbf{X}_{imu} = [\mathbf{p}_{imu}, \mathbf{v}_{imu}]^T$ . In other words, the TT II robot has two separate sources of sensory body state data,  $\mathbf{X}_{JC}$  and  $\mathbf{X}_{imu}$ .

## B. Noise Analysis And Regression Fitting

In general, measurement noise and process noise are assumed to follow a Gaussian distribution, and their covariance matrices are often set as constant in state estimation. However, due to the complexity of bipedal system, the process covariance matrix often varies over time. Moreover, when the robot is equipped with the ESVC foot, its model error also affects the noise distribution. Therefore, in this section, we analyze the noise characteristics and determine the distribution of the robot with the ESVC foot through two experiments.

1) *Analysis of Measurement Noise*: Measurement noise is composed of the multiple sensors noise. For the two separate sources of sensory body state data of TT II, we use  $\sigma_{imu}^2 = [\sigma_{posimu}^2, \sigma_{velimu}^2]$  and  $\sigma_{JC}^2 = [\sigma_{posJC}^2, \sigma_{velJC}^2]$  to denote the measurement variance. The target trajectory of FP is designed to follow a path resembling the Lemniscate of Bernoulli. In the joint space, the actuators are controlled to accurately track the target joint position trajectory generated by the ESVC inverse kinematics. Several marker points are placed to indicate the positions of various body links of the robot, and a depth camera is employed to capture the joint angles.

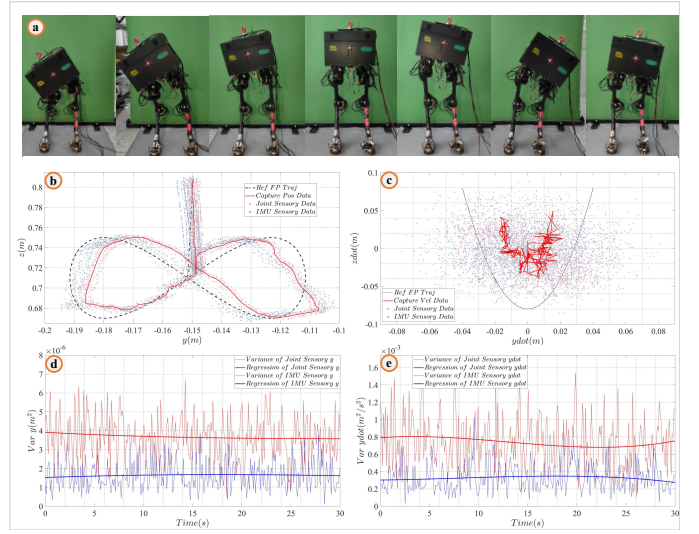


Fig. 1. (a). Snapshots FP trajectory tracking physical experiments on robot TT II. (b). Coronal FP position trajectory over ten experiments. (c). Coronal FP velocity trajectory over ten experiments. (d). FP position error variance distribution. (e). FP velocity error variance distribution.

To minimize the influence of mechanical clearances and motor backlash on measurement noise, the FP target trajectory is constrained to the coronal plane. As a result, the feet exhibit displacement only along the Y-axis and rotation about the X-axis. Although the foot roll angle is relatively small, its effect on the FP point cannot be neglected due to amplification caused by the supporting leg length. Finally, the position and velocity of the FP relative to the fixed frame are computed as ground truth using the URDF model, with two additional virtual joints introduced of the motion of Y-axis and X-axis.

Snapshots of the robot physical experiments are shown in Fig1.a. To eliminate random errors, the same experiment was repeated ten times, and the position and velocity of the FP in the coronal plane are depicted in Fig1.b and Fig1.c. The red points represent the sensory data from the configuration space, while the blue points indicate the data obtained from IMU integration. The dashed line denotes the reference trajectory and the solid lines show the ground truth obtained from the depth camera data. From the figure we find that the measurement noise exhibits characteristics of a Gaussian distribution. The variance vector  $\sigma^2$  of the two sensory body state data are computed using Eq.3.  $\mathbf{X}_{FPi}$  and  $\hat{\mathbf{X}}_{FPi}$  represent the ground truth and the measured state from sensory data of FP trajectory, respectively. Since the two sets of sensory state data are computed in the same manner, we use  $\sigma_{imu0}^2$  and  $\sigma_{JC0}^2$  to distinguish between them. We calculate the variance of measurement errors in position and velocity along the Y and Z directions at time intervals of 0.01 seconds, as shown in Fig1.d and Fig1.e. It can be observed from the figure that the measurement noise still remains nearly constant over time. Similar results can also be observed in the X direction. Therefore, the covariance matrices and of the two sensory state data of TT II robot can be approximated as constant diagonal matrices  $\sigma_{imu0}^2$  and  $\sigma_{JC0}^2$ , respectively, and their values can

be determined accordingly.

$$\sigma^2 = \frac{1}{n-1} \sum_{i=1}^n \left( \mathbf{X}_{FPi} - \hat{\mathbf{X}}_{FPi} \right)^2 \quad (3)$$

**2) Analysis of Process Noise:** Process noise is typically caused by mechanical clearances, motor backlash, and model inaccuracies. For bipedal robots with the ESVC foot, the elliptical arc length lacks a closed-form solution. To address this, our prior work introduced an approximation calculation based on elementary-function. However, the approximation errors in velocity and position are magnified by the leg length, thereby compromising the accuracy of body state estimation. Therefore, before designing the state estimator, it is essential to analyze the noise introduced by the ESVC foot and determine its distribution.

Open-loop marking time experiments on the TT II robot were conducted to investigate how modeling errors of the ESVC foot affect the system process noise. We first generate the desired CoM and swing foot target state trajectories using the HLIP model [25]. Since the ESVC foot operates in coronal plane, the approximate kinematic model is used to formulate contact point position constraints and friction cone constraints. These are incorporated into a full-order trajectory optimization based on DIRCON [27] to generate the desired joint trajectories. The orientation of swing foot is constrained to maintain parallel with the ground at all times. For HLIP model, the duration of single support phase is 0.42s and the orbit composition is SP1-CP2. The nominal step length during the left support phase(LSP) is  $-0.303\text{m}$ , which aligns with the relative positions of the left and right feet when the robot is in static standing posture. The target joint positions, velocities, and feedforward torques are obtained by solving the optimization and the robot is controlled to track the trajectories using PD feedforward control and gravity compensation. To ensure experimental repeatability, the TT II robot is initialized to a fixed posture by a calibration device, and then performs marking time by tracking the target joint trajectories, as depicted in Fig2.a. Of course, the robot inevitably tilts and falls over time. For analysis, we focus on several steps exhibiting relatively accurate tracking. The reference joint position and data are obtained by the depth camera while the orientation and angular velocity of the support foot are directly measured by an inclinometer and gyroscope mounted at the center of the foot upper plane. The event of support phase transition is determined by the onboard timer. Then the CoM state w.r.t contact point frame is calculated through forward kinematics with URDF file and ESVC foot model(Eq.2). Sixteen identical experiments were conducted to collect sample data. For clarity, a sampling interval of 0.08 seconds was used. The Y-direction position and velocity of five steps with better performance are plotted in Fig2.b and Fig2.c, respectively, where the color variation of each point indicates the corresponding sampling time.

It can be observed that even with the ESVC foot, the Y-direction position and velocity of the CoM approximately follow a normal distribution with clearly time-dependent characteristics. Similar results can also be observed in the X and Z directions. Moreover, significant discrepancies exist between

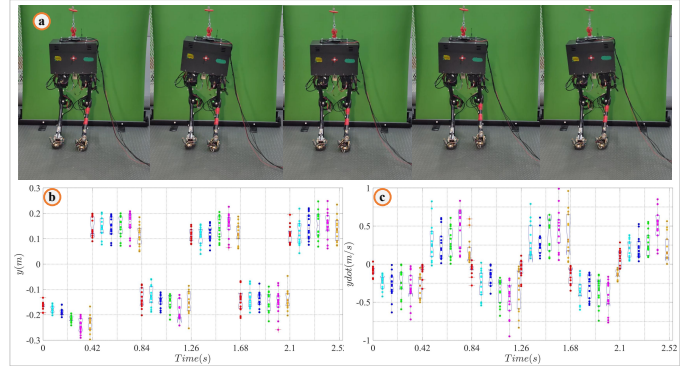


Fig. 2. (a) Snapshots of TT II marking time. (b) FP position trajectories over 16 experiments. (c) FP velocities trajectories over 16 experiments.

the experimental and theoretical trajectories in both velocity and direction, indicating that the TT II robot experiences relatively large process noise. Another noteworthy observation is that, for the Y-direction velocity, the measured data and the theoretical trajectory exhibit opposite signs at each step transition. For instance, the red points at the beginning of the third step in Fig2.c correspond to the transition from the RSP and LSP. Theoretically, the FP velocity in the Y direction should be positive at these transitions; however, the feedback data from the robot show a negative velocity, indicating that the swing foot made premature contact with the ground. Nevertheless, since the magnitude of the velocity is small, this indicates a premature contact of the swing foot.

**3) Regression of Process Noise:** To suppress the influence of incidental fluctuations, we first compute the average trajectory over the six selected steps. As the data storage frequency of robot system is 1kHz, each step for a single experiment will yield 420 data points. We divide the data points into 9 segments: the first eight segments each last 0.05s, and the final segment has a duration of 0.02s. Then the data from the six steps are subsequently merged into a single step, and the error variance trajectory of both CoM state is calculated accordingly. To analyze the error variance, the error variance trajectory is further divided into multiple sub-segments with each containing 20 knots and different weights are assigned to the variance points. Each sub-segment is referred to as a weighted variance window. The first eight segments are each associated with five weighted windows, whereas the final segment contains two. The variance at the center of each window is taken as the representative value of that window. By performing cubic polynomial regression to the representative values of these windows, the characteristics and variations of the process noise error variance within a single step can be clearly observed.

For a single weighted window, each variance point is assigned a weight based on its time offset from the segment endpoint, and the central value of the window is updated as

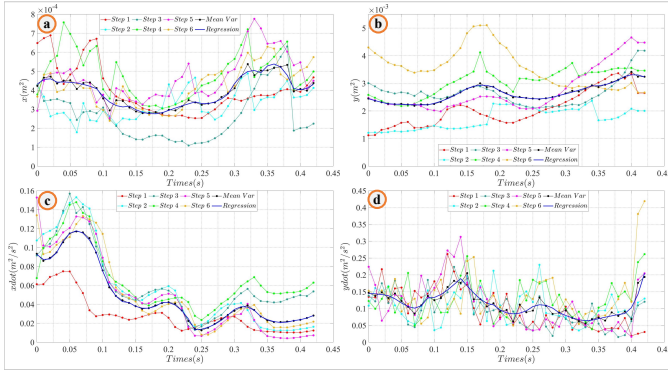


Fig. 3. Process error variance and regression results of TT II walking with ESVC foot over 16 experiments.

follows:

$$\begin{cases} \bar{y}_k = \frac{1}{N} \sum_{n=1}^N w_{k,n} y_{k,n} \\ w_{k,n} = e^{-\frac{(t_n - t_k)^2}{2\tau_w^2}} \end{cases} \quad (4)$$

$k$  is the index of current window.  $\bar{y}_k$  and  $y_{k,n}$  represent the representative value and the other data samples within the window, respectively.  $t_k$  and  $t_n$  are the corresponding time of  $\bar{y}_k$  and  $y_{k,n}$ .  $w_{k,n}$  is the weights of each point derived from Gaussian kernel function and  $\tau_w$  is smoothing parameter.

After processing the data, we used a regression model to extract temporal variation features. For the 9 data segments, the cubic polynomial regression is performed on window center value vector  $\bar{\mathbf{y}}_j$ . The resulted regression expression can be characterized as:

$$g_j = a_{j-1}t^3 + a_{j-2}t^2 + a_{j-3}t + a_{j-3} \quad (5)$$

$j$  is the index of the segment and  $g_j$  is the fitted value.  $t$  is the current sample time.  $\mathbf{a}_j = [a_{j-1}, a_{j-2}, a_{j-3}, a_{j-3}]^T$  represents the cubic parameters of current segment and can be calculated as:

$$\mathbf{a}_j = (\mathbf{t}_j^T \mathbf{t}_j)^{-1} \mathbf{t}_j^T \bar{\mathbf{y}}_j \quad (6)$$

$\mathbf{t}_j$  is the vector containing the sampling times of all window centers within this segment.

For different segments, a first-order continuity constraint is also enforced. Then the process error variances of the CoM position and velocity in both the X and Y directions are depicted in Fig3. The black curves denote the average variance of the selected steps and the blue curves represents the regression result. As shown in the figure, the process noise error variance in both the X and Y directions is strongly time-dependent, with trends that are smooth and easily fitted. This observation supports the development of state estimators and performance enhancement methods for robots employing the ESVC foot.

### III. HIERARCHICAL ADAPTIVE BODY STATE ESTIMATOR

In the previous section, we analyzed the impact of the ESVC foot on system noise of the TT II robot through physical FP tracking and marking time experiments. For the measurement

noise, it exhibited approximately constant error variance over time. For the process noise, we confirmed that despite the modeling errors introduced by the ESVC foot, it still approximately follows a normal distribution. This validates the use of a Gaussian model for characterizing the robot process noise, which is crucial for designing state estimators for bipedal robots with the ESVC foot. Based on these findings, this section presents the proposed adaptive state estimator.

The proposed body state estimator contains two layers. In the first layer, a pre-estimate of the robot sensory data is obtained based on fusion methods. For the second layer, an adaptive variation of extended Kalman filter(EKF) is employed to further update the CoM state with the temporal regression model.

#### A. Data Fusion Based Pre-Estimation

As described in secII, the TT II robot provides two types of direct sensory state,  $\mathbf{X}_{imu}$  and  $\mathbf{X}_{JC}$ . In this section, we use  $\check{\mathbf{X}}_i = [\check{\mathbf{p}}_i, \check{\mathbf{v}}_i]$  to represent the data at  $t_i$  after pre-estimation. Due to the significant differences between position and velocity errors, they are treated separately. For position, we directly fuse the two types of sensory position from the robot:

$$\check{\mathbf{p}}_i = \mathbf{p}_{JC.i} + \mathbf{K}_{pos}(\mathbf{p}_{imu.i} - \mathbf{p}_{JC.i}) \quad (7)$$

$\mathbf{K}_{pos}$  is a position fusion diagonal matrix composed of  $K_{posx}$ ,  $K_{posy}$  and  $K_{posz}$ . The optimal fusion parameter can be easily obtained by Eq.8:

$$\mathbf{K}_{pos.i} = \frac{\sigma_{JC.i}^2}{\sigma_{imu.i}^2 + \sigma_{JC.i}^2} \quad (8)$$

The error variance vector after fusing is  $\check{\sigma}_{prepos} = [\check{\sigma}_{prex}, \check{\sigma}_{prey}, \check{\sigma}_{prez}]^T$ . Since the two sensory data of the robot are decoupled, the parameters of position fusion are:

$$\check{\sigma}_{prepos}^2 = \begin{bmatrix} (1 - K_{posx})^2 & K_{posx}^2 \\ (1 - K_{posy})^2 & K_{posy}^2 \\ (1 - K_{posz})^2 & K_{posz}^2 \end{bmatrix} [\sigma_{JCpos}^2 \quad \sigma_{imupos}^2]^T \quad (9)$$

For velocity, since experimental observations indicate that joint velocity encoder errors increase significantly under vibrations, a two-step data fusion strategy is adopted. First, we construct a differential velocity  $\mathbf{v}_{diff.i}$  through  $\check{\mathbf{p}}$ :

$$\mathbf{v}_{diff.i} = \frac{\check{\mathbf{p}}_i - \check{\mathbf{p}}_{i-1}}{\sigma t} \quad (10)$$

$\sigma t$  is the sampling interval and the variance of  $\mathbf{v}_{diff.i}$  can be compute as:

$$\check{\sigma}_{diff}^2 = \begin{bmatrix} (1 - K_{posx})^2 & K_{posx}^2 \\ (1 - K_{posy})^2 & K_{posy}^2 \\ (1 - K_{posz})^2 & K_{posz}^2 \end{bmatrix} \begin{bmatrix} \sigma_{posJC}^2 & \sigma_{posimu}^2 \end{bmatrix}^T \quad (11)$$

At first step, we fuse  $\mathbf{v}_{diff.i}$  and  $\mathbf{v}_{imu.i}$  as shown in Eq.12. The corresponding fusion diagonal matrix  $\check{\mathbf{K}}_{vel}$  and error variance  $\check{\sigma}_{vel}^2$  is calculated analogously to  $\mathbf{K}_{pos}$  and  $\check{\sigma}_{pos}^2$ ,

as illustrated in Eq.12 and Eq.13.

$$\begin{cases} \bar{\mathbf{v}}_i = \mathbf{v}_{diff,i} + \bar{\mathbf{K}}_{vel}(\mathbf{v}_{imu,i} - \mathbf{v}_{diff,i}) \\ \bar{\mathbf{K}}_{vel} = \frac{\sigma_{diff}^2}{\sigma_{diff}^2 + \sigma_{velimu}^2} \end{cases} \quad (12)$$

$$\bar{\sigma}_{vel}^2 = \begin{bmatrix} (1 - K_{velx})^2 & K_{velx}^2 \\ (1 - K_{vely})^2 & K_{vely}^2 \\ (1 - K_{velz})^2 & K_{velz}^2 \end{bmatrix} [\sigma_{diff}^2 \quad \sigma_{velimu}^2]^T \quad (13)$$

At second step, the  $\bar{\mathbf{v}}_i$  is fused with joint sensory data  $\mathbf{v}_{JC,i}$  as described in Eq.14.  $\check{\mathbf{v}}_{ci}$  denotes the resulting velocity and  $\check{\mathbf{K}}_{vel}$  represents the fusion matrix. The error variance after second fusion  $\check{\sigma}_{vel}^2$  is depend on  $\bar{\sigma}_{vel}^2$  and  $\sigma_{velJC}^2$ , as shown in Eq.15.

$$\begin{cases} \check{\mathbf{v}}_i = \bar{\mathbf{v}}_{JC,i} + \check{\mathbf{K}}_{vel}(\bar{\mathbf{v}}_i - \mathbf{v}_{JC,i}) \\ \check{\mathbf{K}}_{vel} = \frac{\sigma_{JC,i}^2}{\sigma_{JC,i}^2 + \bar{\sigma}_{vel}^2} \end{cases} \quad (14)$$

$$\check{\sigma}_{vel}^2 = \begin{bmatrix} (1 - K_{velx})^2 & K_{velx}^2 \\ (1 - K_{vely})^2 & K_{vely}^2 \\ (1 - K_{velz})^2 & K_{velz}^2 \end{bmatrix} [\bar{\sigma}_{vel}^2 \quad \sigma_{velJC}^2]^T \quad (15)$$

### B. Adaptive post-Estimation

For the post-Estimation, the CoM state in X direction is denoted as  $\mathbf{X}_{comx,i} = [p_{x,i}, v_{x,i}]^T$  and its state transition equation and observation equation can be written as:

$$\begin{cases} \mathbf{X}_{comx,i+1} = \begin{bmatrix} 1 & \sigma t & \sigma t^2 \\ 0 & 1 & \sigma t \end{bmatrix} [\mathbf{X}_{comx,i} \quad \check{\mathbf{a}}_{x,i} + \boldsymbol{\omega}_i]^T \\ \mathbf{Z}_{comx,i+1} = \mathbf{H}_x [\check{p}_{comx,i} \quad \check{v}_{comx,i} + \phi_i]^T \end{cases} \quad (16)$$

$\check{\mathbf{a}}_{x,i}$  is the X direction component of the CoM acceleration  $\check{\mathbf{a}}_i$ .  $\mathbf{H}_x$  is the observation matrix and  $\mathbf{Z}_{comx,i+1}$  is the measurement state.  $\boldsymbol{\omega}_i$  and  $\phi_i$  represent the process noise and measurement noise, respectively. Before we perform EKF to Eq.16, the acceleration of CoM,  $\check{\mathbf{a}}_{x,i}$  should be determined. Although it is feasible to compute the CoM acceleration directly from foot contact forces and joint accelerations, modeling inaccuracies introduce errors in the results which will be infeasible for integration. Moreover, for the robot without contact force sensor, such as TT II and Cassie, the contact force need additional estimation that also increase the computational burden on the onboard system. It is worth noting that, since the robot is constrained to follow the HLIP model during walking, its CoM acceleration should closely match that of the HLIP behaviour. From another point, as an IMU is located at FP is close to the CoM, the sensor data can also be used to approximate the CoM acceleration. Then the acceleration of CoM can be obtained by fusing the acceleration of HLIP model and FP point:

$$\check{\mathbf{a}}_i = \mathbf{a}_{fp,i} + \mathbf{K}_a(\mathbf{a}_{hlip} - \mathbf{a}_{fp,i}) \quad (17)$$

$\mathbf{a}_{hlip} = \left[ \frac{\check{p}_{xi}}{h_0}, \frac{\check{p}_{yi}}{h_0}, 0 \right]^T$  is the theoretical acceleration of HLIP.  $\check{p}_{xi}$  and  $\check{p}_{yi}$  are the CoM position w.r.t. contact position.  $h_0$  is the target CoM height.  $\mathbf{K}_a$  is the fusion diagonal matrix composed of  $K_{ax,i}$ ,  $K_{ay,i}$  and  $K_{az,i}$ . As the CoM state approaches the theoretical model state, the HLIP acceleration

becomes more reliable, i.e.,  $\mathbf{K}_a$  tends toward 0. Conversely, when the CoM state deviates further from the model state, we place greater trust in the acceleration measured at the FP point. Therefore, a Gaussian kernel function is chosen to determine  $K_{ax,i}$ . Taking the X-direction as an example:

$$K_{ax,i} = e^{-\frac{(\bar{p}_{x,i} - p_{hx,i})^2 + (\bar{v}_{x,i} - v_{hx,i})^2}{2\tau_a^2}} \quad (18)$$

$p_{hx,i}$  and  $v_{hx,i}$  is the desired CoM state of HLIP,  $\tau_a$  is the smoothing parameter. At this point, both the state transition equation and observation equation in Eq.16 are fully defined.

As discussed in SecII, both measurement noise and process noise are approximately follow a Gaussian distribution and the error covariance matrices can be predicted at any time through the temporal regression model. It is important to note that the regression model is established based on the FP trajectory tracking task and the marking time task. In practice, when the robot changes its behavior, such as variations in walking speed or CoM height, the characteristics of both measurement noise and process noise should also change. Consequently, the error covariance matrices also need to be updated in time. In other words, it is impractical to analyze the noise characteristics for all possible robot motions and the post-estimation is required to adaptively update the covariance matrices. For bipedal robots, squatting and walking serve as templates for more complex motions. Therefore, the regression model derived from noise analysis can serve as an initial estimate for updating the current covariance matrices, and the subsequent updates will rollover with the historical covariance matrices. The measurement noise covariance and process noise covariance are updated as:

$$\begin{cases} \tilde{\mathbf{R}}_{C,i} = \alpha \mathbf{R}_{C,i} + (\mathbf{I} - \alpha) \hat{\mathbf{R}}_{C,i} \\ \tilde{\mathbf{Q}}_{C,i} = \beta_0 \mathbf{Q}_{C,i} + \beta_1 \hat{\mathbf{Q}}_{C,i} + \beta_2 \tilde{\mathbf{Q}}_{C,i-1} \end{cases} \quad (19)$$

$\tilde{\mathbf{R}}_{C,i}$  and  $\tilde{\mathbf{Q}}_{C,i}$  are the updated error covariance matrices of measurement noise and process noise, respectively, while  $\mathbf{R}_{C,i}$  and  $\mathbf{Q}_{C,i}$  represent the initial estimate covariance matrices which are initialized by  $\mathbf{R}_{C,0}$  and  $\mathbf{Q}_{C,0}$  from SecII.  $\hat{\mathbf{R}}_{C,i}$  and  $\hat{\mathbf{Q}}_{C,i}$  are estimated from the variance of residuals. For simplicity, we directly use the squared residuals. For the temporal characteristics of the process noise, the covariance matrix from the previous time step is used as the third term in the update loop.  $\alpha \in \mathbb{R}^{6 \times 6}$  is a constant measurement update parameter matrix, corresponding to the three-dimensional position and velocity of the CoM,  $\beta_0$ ,  $\beta_1$  and  $\beta_2$  are the process update parameter matrix which denotes the weights of initial estimate covariance matrices, measurement residuals and historical covariance matrix, respectively. And these matrices satisfy the constraint  $\beta_0 + \beta_1 + \beta_2 = \mathbf{I}_6$ . At this point, standard EKF operations can be applied to Eq.16, which are not elaborated here. Then the error variance  $\sigma_{JC,i}^2$  and  $\sigma_{imu,i}^2$  of sensory data still need to be updated, as shown in Eq.20.  $e_{JC,i}$  denotes the difference between CoM state  $\mathbf{X}_{JC,i}$  derived from joint sensory data and the post-estimated state  $\check{\mathbf{X}}_i$  and the update of  $\sigma_{imu,i}^2$  follows the same procedure as that of  $\sigma_{JC,i}^2$ . At the beginning of robot motion,  $\sigma_{imu,i}^2$  and

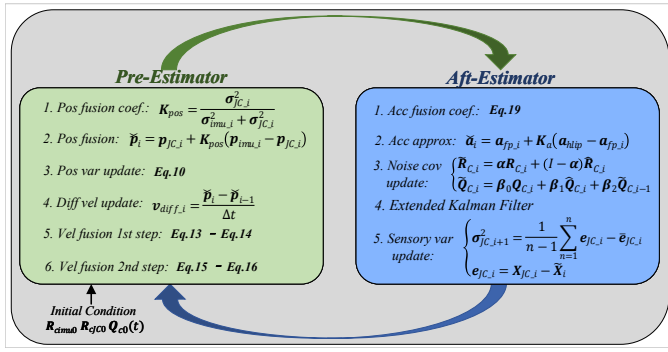


Fig. 4. The overall architecture of the proposed hierarchical body state estimator.

$\sigma_{JC_i}^2$  are initialized using  $\sigma_{imu0}^2$  and  $\sigma_{JC0}^2$ , respectively.

$$\begin{cases} \sigma_{JC,i+1}^2 = \frac{1}{n-1} \sum_{n=1}^N e_{JC,i}^2 - \bar{e}_{JC,i} \\ e_{JC,i} = X_{JC,i} - \tilde{X}_i \end{cases} \quad (20)$$

For clarity, the proposed hierarchical body state estimator is illustrated in Fig4. Components with a green background represent the data fusion-based pre-estimation stage, while those with a blue background correspond to the adaptive post-estimation.

## IV. EXPERIMENT EVALUATION

### A. Experimental Setup

To evaluate the proposed body state estimator, two types of physical experiments were conducted on the TT II robot: marking time and variable-speed lateral walking. The joints of TT II are actuated by AK-8064, a high-power motor designed by Cubemars [28]. The onboard computer is an Intel i7-8665U processor running Xenomai 3.2 real-time Linux as the main controller. The robot communication network is based on CAN network and all the sensory data are returned by HWT-9073-CAN developed by WIT MOTION [29]. Each ESVC foot is equipped with four pressure sensors for contact detection. The robot is controlled to follow the HLIP model, with the swing foot trajectory generated using cubic Hermite spline. The target joint space trajectory is synthesized through optimization-based phased inverse kinematics(PIK) and solved by the DRAKE robotics toolbox [30]. The actuated joints track the reference trajectory via PD control with feedforward compensation.

### B. Marking Time

To verify the accuracy of the estimator, marking time experiment was conducted on the TT II robot and the snapshots of a complete step is shown in Fig5.a. Acquiring the true states of a dynamic system is inherently challenging and an approximate ground truth is established by capturing joint kinematic data with a depth camera and reflective markers. Then the CoM trajectory using forward kinematics derived from the URDF model. The CoM phase portrait of Y-direction and Z-direction are shown in Fig5.b and Fig5.c, respectively.

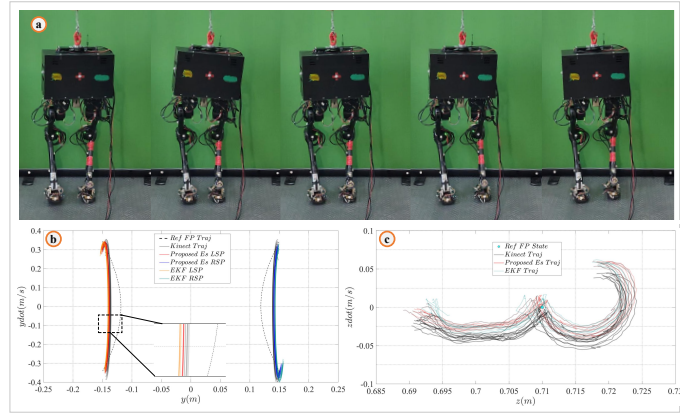


Fig. 5. (a). The snapshots of marking time experiment with TT II; (b). CoM phase portrait of Y-direction; (c). CoM phase portrait in Z-direction.

The black dashed line represents the reference trajectory of the HLIP model, while the dark gray solid line denotes the ground truth of the walking center of mass. The red and blue curves represent the feedback data estimated by the proposed method, corresponding to the left support phase and the right support phase. From the figure, it can be observed that the CoM states estimated by the proposed method closely approximate the ground truth during marking time. However, due to inherent measurement errors, the vision-based feedback also deviates to some extent from the true values. To provide a comparative baseline, we also introduce the EKF, as indicated by the orange and sky blue curves in Fig5.b and Fig5.c. Through comparison, it is observed that the proposed estimator can stably provide accurate state estimates during robot locomotion, with slightly better performance than the EKF-based method.

### C. Variable-speed Lateral Walking

To evaluate the performance of the state estimator under more complex locomotion conditions, a variable-speed lateral walking experiment was conducted. The TT II robot was controlled to decelerate from lateral walking at 0.1m/s to marking time, and then accelerate to a lateral walking speed of 0.2m/s, as illustrated in Fig6. Given the increased difficulty in obtaining accurate ground truth during dynamic walking, the EKF-based estimation is adopted as the reference baseline for comparison in this section. To further evaluate the adaptability of the proposed state estimator, the Adaptive EKF(AEKF) is also included as a baseline for comparison. The number of steps required for the robot to reach stable walking is used as the evaluation criterion. To highlight the influence of the ESVC foot, the variation of the CoM position in the Y-direction over time is plotted in Fig6. The red and blue curves represent the state estimates obtained by the proposed method during the LSP and RSP phases, respectively. The EKF results are shown in orange and sky blue, while the Adaptive EKF (AEKF) estimates are depicted in brown and navy blue. Through observation, we find that during steady walking, all three estimators exhibit comparable accuracy, and their outputs are sufficient to enable stable walking of the robot equipped with the ESVC foot. In the acceleration and deceleration phases, the convergence performance of the three

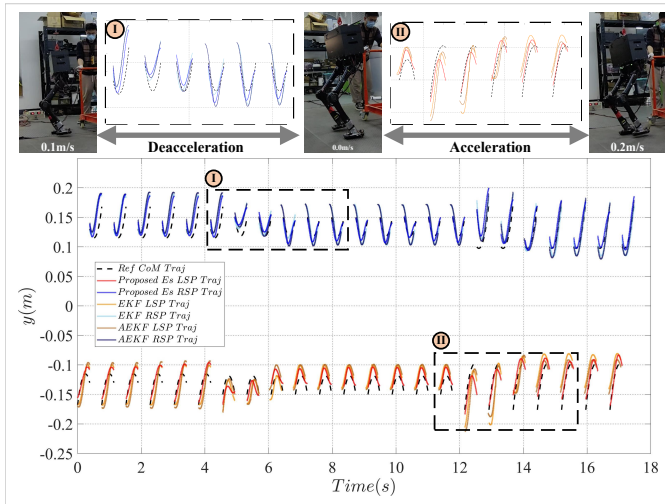


Fig. 6. Performance evaluation of EKF, AEKF and proposed estimator through CoM position in Y-direction.

estimators varies significantly. The trajectories corresponding to the acceleration and deceleration phases are magnified and presented in the upper section of Fig6. In the deceleration phase, the HLIP theoretical model plans the transition within two steps. In contrast, the robot employing the proposed estimator completed the deceleration over four steps, primarily due to modeling inaccuracies and residual estimation errors relative to the true states. The AEKF-based method also completed the deceleration during the fourth LSP, whereas the EKF required until the sixth RSP step to complete the transition. This indicates that both the proposed state estimator and the AEKF exhibit faster convergence than the EKF. In the acceleration phase, the robot using the proposed estimator reached the target stable state also within four steps, while both the AEKF and EKF required six steps to achieve stability. This demonstrates that the proposed estimator achieves faster convergence and, consequently, exhibits better adaptability compared to both EKF and AEKF.

## V. CONCLUSION

This paper investigates body state estimation for bipedal robots equipped with an ESVC (Ellipse-based Segmental Varying Curvature) foot—a bioinspired design that improves gait efficiency but introduces modeling uncertainties due to complex foot–ground interactions. Physical experiments are conducted to determine the distribution of measurement and process noise, and a time-varying fitting model of covariance matrix is constructed via weighted cubic polynomial regression. A hierarchical adaptive estimator is proposed, consisting of a multi-sensor data fusion–based pre-estimation stage and an adaptive post-estimation stage. In physical marking-time and variable-speed lateral walking, the proposed state estimation method delivers performance comparable to that of the AEKF and slightly better than the EKF. Moreover, when the robot’s motion changes, the proposed estimator demonstrates superior adaptability compared to both EKF and AEKF.

## REFERENCES

- [1] G1 Biped Robot. Available: <https://www.unitree.com/cn/g1>.
- [2] Atlas Biped Robot. Available: <https://bostondynamics.com/atlas>.
- [3] Digit Biped Robot. Available: <https://www.agilityrobotics.com/solution>.
- [4] R. H. Crompton, W. Sellers, K. Davids, J. McClymont, "Biomechanics and the origins of human bipedal walking: The last 50 years." *Journal of biomechanics*, vol. 157, p. 111701, 2023.
- [5] I. Frizza, K. Ayusawa, A. Cherubini, H. Kaminaga, P. Fraisse, and G. Venture, "Humanoids' feet: State-of-the-art & future directions," *International Journal of Humanoid Robotics*, vol. 19, no. 1, Mar. 2022, Art. no. 2250001.
- [6] A. Smyrli, M. Ghiassi, A. Kecskeméthy, and E. Papadopoulos, "On the effect of semielliptical foot shape on the energetic efficiency of passive bipedal gait," *IEEE/RSJ International Conference on Intelligent Robots and Systems (IROS)*, Macau, China, pp. 6302–6307, Nov. 2019.
- [7] A. Smyrli and E. Papadopoulos, "Modeling, Validation, and Design Investigation of a Passive Biped Walker with Knees and Biomimetic Feet," *2022 International Conference on Robotics and Automation (ICRA)*, Philadelphia, PA, USA, pp. 193–199, 2022.
- [8] J. Li, Y. Tian, X. Huang, and L. Wang, "Foot shape for passive dynamic kneed biped robot," *IEEE International Conference on Robotics and Biomimetics (ROBIO)*, pp. 1281–1286, Dec. 2010.
- [9] L. Han, X. Chen, Z. Yu, X. Zhu, K. Hashimoto, and Q. Huang, "Trajectory-free dynamic locomotion using key trend states for biped robots with point feet," *Science China Information Sciences*, vol. 66, Aug. 2023, Art. no. 189201.
- [10] Z. Liu, J. Gao, X. Rao, S. Ding, and D. Liu, "Complex dynamics of the passive biped robot with flat feet: Gait bifurcation, intermittency and crisis," *Mechanism and Machine Theory*, vol. 191, Jan. 2024, Art. no. 105500. Available: <http://www.bookref.com>.
- [11] G. García, R. Griffin, and J. Pratt, "MPC-based locomotion control of bipedal robots with line-feet contact using centroidal dynamics," *Humanoids*, Munich, Germany, pp. 1–8, Jul. 2021.
- [12] Our previous paper Model Analysis And Design Of Ellipse Based Segmented Varying Curved Foot For Biped Robot Walking.
- [13] B. Li, G. Xu, Z. Teng, et al., "Intelligent ankle–foot prosthesis based on human structure and motion bionics," *Journal of NeuroEngineering and Rehabilitation*, vol. 21, no. 1, Jan. 2024, Art. no. 119.
- [14] C. Piazza, C. Della Santina, G. M. Gasparri, and A. Bicchi, "Toward an adaptive foot for natural walking," in *Proceedings of the 2016 IEEE-RAS 16th International Conference on Humanoid Robots (Humanoids)*, Cancun, Mexico, pp. 1204–1210, Nov. 2016.
- [15] L. Ren, D. Howard, L. Ren, C. Nester, and L. Tian, "A generic analytical foot rollover model for predicting translational ankle kinematics in gait simulation studies," *Journal of Biomechanics*, vol. 43, no. 2, pp. 194–202, Jan. 2010.
- [16] P. Mahmoodi, R. S. Ransing, and M. I. Friswell, "Modelling the effect of 'heel to toe' roll-over contact on the walking dynamics of passive biped robots," *Applied Mathematical Modelling*, vol. 37, no. 12–13, pp. 7352–7373, Jun. 2013.
- [17] Q. Mei, H. K. Kim, L. Xiang, V. Shim, A. Wang, J. S. Baker, Y. Gu, and J. Fernandez, "Toward improved understanding of foot shape, foot posture, and foot biomechanics during running: A narrative review," *Frontiers in Physiology*, vol. 13, pp. 1–12, Dec. 2022, Art. no. 1062598.
- [18] T. Mikołajczyk, E. Mikołajewska, H. F. N. Al-Shuka, T. Malinowski, A. Klodowski, D. Y. Pimenov, T. Paczkowski, F. Hu, K. Giasin, D. Mikołajewski, and M. Macko, "Recent advances in bipedal walking robots: Review of gait, drive, sensors and control systems," *Sensors*, vol. 22, no. 12, pp. 1–31, Jun. 2022, Art. no. 4440.
- [19] C.-P. Chen, J.-Y. Chen, C.-K. Huang, J.-C. Lu, and P.-C. Lin, "Sensor data fusion for body state estimation in a bipedal robot and its feedback control application for stable walking," *Sensors*, vol. 15, no. 3, pp. 4925–4946, Feb. 2015.
- [20] J. Kang, Y. Wang, and X. Xiong, "Fast decentralized state estimation for legged robot locomotion via EKF and MHE," *IEEE Robotics and Automation Letters*, vol. 9, no. 12, pp. 1–8, Dec. 2024, Art. no. 3483043.
- [21] T.-Y. Lin, R. Zhang, J. Yu, and M. Ghaffari, "Legged robot state estimation using invariant Kalman filtering and learned contact events," *arXiv preprint arXiv:2106.15713*, Jun. 2021.
- [22] C. Gao, Y. Xie, S. Zhu, and Y. Wang, "Adaptive robust invariant extended Kalman filtering for biped robot," in *Proceedings of the 2022 IEEE International Conference on Robotics and Biomimetics (ROBIO)*, Xishuangbanna, China, pp. 1885–1891, Dec. 2022.
- [23] H. Kim, S. Hong, G. Ji, S. Jeon, J. Hwangbo, J.-H. Oh, and H.-W. Park, "Legged robot state estimation with dynamic contact event information,"

- IEEE Robotics and Automation Letters, vol. 6, no. 4, pp. 6733–6740, Oct. 2021.
- [24] D. Youm, H. Oh, S. Choi, H. Kim, and J. Hwangbo, “Legged robot state estimation with invariant extended Kalman filter using neural measurement network,” arXiv preprint arXiv:2402.00366, Feb. 2024.
- [25] X. Xiong, A. Ames, “3-d underactuated bipedal walking via h-hip based gait synthesis and stepping stabilization”. IEEE Transactions on Robotics, vol. 38, no. 4, pp. 2405-2425, Aug. 2022.
- [26] Supplement Data, Available: <https://github.com/cby-gh/Estimation-ESVC-FOOT>
- [27] B. Chen, X. Zang, Y. Zhang, L. Gao, Y. Zhu, and J. Zhao, “A non-flat terrain biped gait planner based on DIRCON,” Biomimetics, vol. 7, no. 4, pp. 1–18, Nov. 2022, Art. no. 203.
- [28] Joint Actuator, Available: <https://www.cubemars.com/cn/goods-1143-AK80-64.html>.
- [29] IMU & Inclinometer, Available: <https://www.wit-motion.com/>.
- [30] Drake, Available: <https://drake.mit.edu/>.

# Preparation of Papers for IEEE TRANSACTIONS and JOURNALS (May 2024)

First A. Author, *Fellow, IEEE*, Second B. Author, and Third C. Author, Jr., *Member, IEEE*

**Abstract**—The ESVC foot (Ellipse-based Segmental Varying Curvature foot), a robot foot design inspired by the rollover shape of the human foot, significantly enhances the efficiency of the robot's walking gait. However, due to the tilt of the supporting leg, errors in the varying contact model are amplified, making robot state estimation more challenging. Therefore, this paper focuses on the noise analysis and state estimation for robot walking with the ESVC foot. First, through physical robot experiments, we investigate the effect of the ESVC foot on robot process noise and measurement noise. and a noise-time regression model using sliding window strategy is developed. Then, a hierarchical adaptive state estimator for biped robots with the ESVC foot is proposed. The state estimator consists of two stages: pre-estimation and post-estimation. In the pre-estimation stage, a data fusion-based method is employed to process the sensory data. During post-estimation, the CoM(Center of Mass) acceleration is first estimated and then the noise covariance matrices are adjusted based on the regression model. Following that, an EKF(Extended Kalman Filter) based approach is applied to estimate the centroid state during robot walking. Physical experiments demonstrate that the proposed state estimation method for biped robot walking with the ESVC foot not only provides higher precision than both EKF and AEKF, but also converges faster under varying noise conditions.



**Index Terms**—Enter key words or phrases in alphabetical order, separated by comma. Examples: artificial neural network (ANN), circuit parameter extraction, multistatic localization, nonradiative dielectric (NRD) waveguide, numerical calibration waveguide filter, optimal sensor placement, traveling wave antenna.

## I. INTRODUCTION

THIS document is a template for  $\LaTeX$ . If you are reading a paper or PDF version of this document, please download the full  $\LaTeX$  template of your publication choice from the IEEE Web site at <https://template-selector.ieee.org/secure/templateSelector/publicationType> so you can use it to prepare your manuscript. This IEEE Author Center website link below also provides many useful guides on how to write your papers: <https://journals.ieeeauthorcenter.ieee.org/create-your-ieee-journal-article/create-the-text-of-your-article/ieee-editorial-style-manual/>. You can also explore using the Overleaf editor at <https://www.overleaf.com/blog/278-how-to-use-overleaf-with-ieee-collabratec-your-quick-guide-to-getting-started#>.

This paragraph of the first footnote will contain the date on which you submitted your paper for review. It will also contain support information, including sponsor and financial support acknowledgment. For example, "This work was supported in part by the U.S. Department of Commerce under Grant BS123456."

The next few paragraphs should contain the authors' current affiliations, including current address and e-mail. For example, F. A. Author is with the National Institute of Standards and Technology, Boulder, CO 80305 USA (e-mail: author@boulder.nist.gov).

S. B. Author, Jr., was with Rice University, Houston, TX 77005 USA. He is now with the Department of Physics, Colorado State University, Fort Collins, CO 80523 USA (e-mail: author@lamar.colostate.edu).

T. C. Author is with the Electrical Engineering Department, University of Colorado, Boulder, CO 80309 USA, on leave from the National Research Institute for Metals, Tsukuba, Japan (e-mail: author@nrim.go.jp).

If your paper is intended for a conference, please contact your conference editor concerning acceptable word processor formats for your particular conference.

IEEE will do the final formatting of your paper. If your paper is intended for a conference, please observe the conference page limits.

### A. Abbreviations and Acronyms

Define abbreviations and acronyms the first time they are used in the text, even after they have already been defined in the abstract. Abbreviations such as IEEE, SI, ac, and dc do not have to be defined. Abbreviations that incorporate periods should not have spaces: write "C.N.R.S.," not "C. N. R. S." Do not use abbreviations in the title unless they are unavoidable (for example, "IEEE" in the title of this article).

### B. Other Recommendations

Use one space after periods and colons. Hyphenate complex modifiers: "zero-field-cooled magnetization." Avoid dangling participles, such as, "Using (1), the potential was calculated." [It is not clear who or what used (1).] Write instead, "The potential was calculated by using (1)," or "Using (1), we calculated the potential."

Use a zero before decimal points: "0.25," not ".25." Use "cm<sup>3</sup>," not "cc." Indicate sample dimensions as "0.1 cm × 0.2 cm," not "0.1 × 0.2 cm<sup>2</sup>." The abbreviation for "seconds"

is “s,” not “sec.” Use “Wb/m<sup>2</sup>” or “webers per square meter,” not “webers/m<sup>2</sup>.” When expressing a range of values, write “7 to 9” or “7–9,” not “7~9.”

A parenthetical statement at the end of a sentence is punctuated outside of the closing parenthesis (like this). (A parenthetical sentence is punctuated within the parentheses.) In American English, periods and commas are within quotation marks, like “this period.” Other punctuation is “outside”! Avoid contractions; for example, write “do not” instead of “don’t.” The serial comma is preferred: “A, B, and C” instead of “A, B and C.”

If you wish, you may write in the first person singular or plural and use the active voice (“I observed that . . .” or “We observed that . . .” instead of “It was observed that . . .”). Remember to check spelling. If your native language is not English, please get a native English-speaking colleague to carefully proofread your paper.

Try not to use too many typefaces in the same article. You’re writing scholarly papers, not ransom notes. Also please remember that MathJax can’t handle really weird typefaces.

### C. Equations

Number equations consecutively with equation numbers in parentheses flush with the right margin, as in (1). To make your equations more compact, you may use the solidus (/), the exp function, or appropriate exponents. Use parentheses to avoid ambiguities in denominators. Punctuate equations when they are part of a sentence, as in

$$E = mc^2. \quad (1)$$

Be sure that the symbols in your equation have been defined before the equation appears or immediately following. Italicize symbols ( $T$  might refer to temperature, but  $T$  is the unit tesla). Refer to “(1),” not “Eq. (1)” or “equation (1),” except at the beginning of a sentence: “Equation (1) is . . . .”

### D. $\LaTeX$ -Specific Advice

Please use “soft” (e.g., `\eqref{Eq}`) cross references instead of “hard” references (e.g., (1)). That will make it possible to combine sections, add equations, or change the order of figures or citations without having to go through the file line by line.

Please don’t use the `{eqnarray}` equation environment. Use `{align}` or `{IEEEeqnarray}` instead. The `{eqnarray}` environment leaves unsightly spaces around relation symbols.

Please note that the `{subequations}` environment in  $\LaTeX$  will increment the main equation counter even when there are no equation numbers displayed. If you forget that, you might write an article in which the equation numbers skip from (17) to (20), causing the copy editors to wonder if you’ve discovered a new method of counting.

$\BIBTeX$  does not work by magic. It doesn’t get the bibliographic data from thin air but from .bib files. If you use  $\BIBTeX$  to produce a bibliography you must send the .bib files to IEEE.

$\LaTeX$  can’t read your mind. If you assign the same label to a subsection and a table, you might find that Table I has been cross referenced as Table IV-B3.

$\LaTeX$  does not have precognitive abilities. If you put a `\label` command before the command that updates the counter it’s supposed to be using, the label will pick up the last counter to be cross referenced instead. In particular, a `\label` command should not go before the caption of a figure or a table.

Do not use `\nonumber` inside the `{array}` environment. It will not stop equation numbers inside `{array}` (there won’t be any anyway) and it might stop a wanted equation number in the surrounding equation.

If you are submitting your paper to a colorized journal, you can use the following two lines at the start of the article to ensure its appearance resembles the final copy:

```
\documentclass[journal,twoside,web]{ieeecolor}
\usepackage{JournalName}
```

## II. UNITS

Use either SI (MKS) or CGS as primary units. (SI units are strongly encouraged.) English units may be used as secondary units (in parentheses). This applies to papers in data storage. For example, write “15 Gb/cm<sup>2</sup> (100 Gb/in<sup>2</sup>).” An exception is when English units are used as identifiers in trade, such as “3½-in disk drive.” Avoid combining SI and CGS units, such as current in amperes and magnetic field in oersteds. This often leads to confusion because equations do not balance dimensionally. If you must use mixed units, clearly state the units for each quantity in an equation.

The SI unit for magnetic field strength  $H$  is A/m. However, if you wish to use units of T, either refer to magnetic flux density  $B$  or magnetic field strength symbolized as  $\mu_0 H$ . Use the center dot to separate compound units, e.g., “A·m<sup>2</sup>.”

## III. SOME COMMON MISTAKES

The word “data” is plural, not singular. The subscript for the permeability of vacuum  $\mu_0$  is zero, not a lowercase letter “o.” The term for residual magnetization is “remanence”; the adjective is “remanent”; do not write “remnance” or “remnant.” Use the word “micrometer” instead of “micron.” A graph within a graph is an “inset,” not an “insert.” The word “alternatively” is preferred to the word “alternately” (unless you really mean something that alternates). Use the word “whereas” instead of “while” (unless you are referring to simultaneous events). Do not use the word “essentially” to mean “approximately” or “effectively.” Do not use the word “issue” as a euphemism for “problem.” When compositions are not specified, separate chemical symbols by en-dashes; for example, “NiMn” indicates the intermetallic compound Ni<sub>0.5</sub>Mn<sub>0.5</sub> whereas “Ni–Mn” indicates an alloy of some composition Ni<sub>*x*</sub>Mn<sub>1–*x*</sub>.

Be aware of the different meanings of the homophones “affect” (usually a verb) and “effect” (usually a noun), “completion” and “compliment,” “discreet” and “discrete,” “principal” (e.g., “principal investigator”) and “principle” (e.g., “principle of measurement”). Do not confuse “imply” and “infer.”

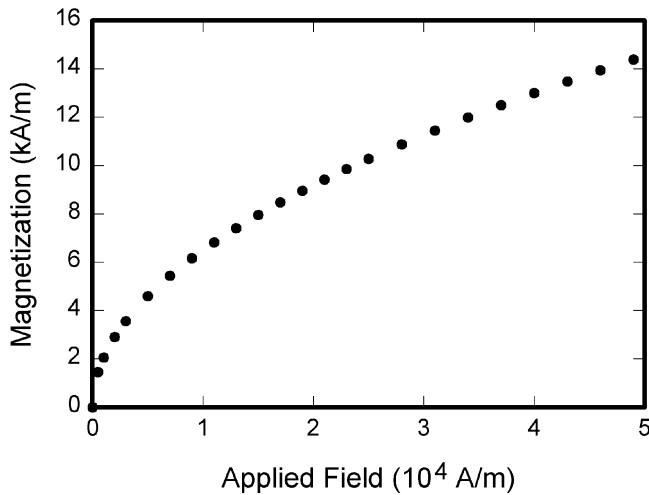


Fig. 1. Magnetization as a function of applied field. It is good practice to explain the significance of the figure in the caption. Inline math example  $E = mc^2$ .

Prefixes such as “non,” “sub,” “micro,” “multi,” and “ultra” are not independent words; they should be joined to the words they modify, usually without a hyphen. There is no period after the “et” in the Latin abbreviation “*et al.*” (it is also italicized). The abbreviation “i.e.,” means “that is,” and the abbreviation “e.g.,” means “for example” (these abbreviations are not italicized).

A general IEEE Editorial Style Manual For Authors is available at <https://journals.ieeeauthorcenter.ieee.org/wp-content/uploads/sites/7/IEEE-Editorial-Style-Manual-for-Authors.pdf>.

## IV. GUIDELINES FOR GRAPHICS PREPARATION AND SUBMISSION

### A. Types of Graphics

The following list outlines the different types of graphics published in IEEE journals. They are categorized based on their construction, and use of color/shades of gray:

1) *Color/Grayscale figures*: Figures that are meant to appear in color, or shades of black/gray. Such figures may include photographs, illustrations, multicolor graphs, and flowcharts.

2) *Line Art figures*: Figures that are composed of only black lines and shapes. These figures should have no shades or half-tones of gray, only black and white.

3) *Author photos*: Head and shoulders shots of authors that appear at the end of our papers.

4) *Tables*: Data charts which are typically black and white, but sometimes include color.

### B. Multipart figures

Figures compiled of more than one sub-figure presented side-by-side, or stacked. If a multipart figure is made up of multiple figure types (one part is lineart, and another is grayscale or color) the figure should meet the stricter guidelines.

TABLE I

UNITS FOR MAGNETIC PROPERTIES. INLINE MATH EXAMPLE:  $E = mc^2$ .

Symbol	Quantity	Conversion from Gaussian and CGS EMU to SI <sup>a</sup>
$\Phi$	magnetic flux	1 Mx $\rightarrow 10^{-8}$ Wb = $10^{-8}$ V·s
$B$	magnetic flux density, magnetic induction	1 G $\rightarrow 10^{-4}$ T = $10^{-4}$ Wb/m <sup>2</sup>
$H$	magnetic field strength	1 Oe $\rightarrow 10^3/(4\pi)$ A/m
$m$	magnetic moment	1 erg/G = 1 emu $\rightarrow 10^{-3}$ A·m <sup>2</sup> = $10^{-3}$ J/T
$M$	magnetization	1 erg/(G·cm <sup>3</sup> ) = 1 emu/cm <sup>3</sup> $\rightarrow 10^3$ A/m
$4\pi M$	magnetization	1 G $\rightarrow 10^3/(4\pi)$ A/m
$\sigma$	specific magnetization	1 erg/(G·g) = 1 emu/g $\rightarrow 1$ A·m <sup>2</sup> /kg
$j$	magnetic dipole moment	1 erg/G = 1 emu $\rightarrow 4\pi \times 10^{-10}$ Wb·m
$J$	magnetic polarization	1 erg/(G·cm <sup>3</sup> ) = 1 emu/cm <sup>3</sup> $\rightarrow 4\pi \times 10^{-4}$ T
$\chi, \kappa$	susceptibility	1 $\rightarrow 4\pi$
$\chi\rho$	mass susceptibility	1 cm <sup>3</sup> /g $\rightarrow 4\pi \times 10^{-3}$ m <sup>3</sup> /kg
$\mu$	permeability	1 $\rightarrow 4\pi \times 10^{-7}$ H/m = $4\pi \times 10^{-7}$ Wb/(A·m)
$\mu_r$	relative permeability	$\mu \rightarrow \mu_r$
$w, W$	energy density	1 erg/cm <sup>3</sup> $\rightarrow 10^{-1}$ J/m <sup>3</sup>
$N, D$	demagnetizing factor	1 $\rightarrow 1/(4\pi)$

Vertical lines are optional in tables. Statements that serve as captions for the entire table do not need footnote letters.

<sup>a</sup>Gaussian units are the same as cg emu for magnetostatics; Mx = maxwell, G = gauss, Oe = oersted; Wb = weber, V = volt, s = second, T = tesla, m = meter, A = ampere, J = joule, kg = kilogram, H = henry.

### C. File Formats For Graphics

Format and save your graphics using a suitable graphics processing program that will allow you to create the images as Tagged Image File Format (.TIFF), Encapsulated PostScript (.EPS), PostScript (.PS), Portable Document Format (.PDF), Portable Network Graphics (.PNG), or Metapost (.MPS), sizes them, and adjusts the resolution settings. When submitting your final paper, your graphics should all be submitted individually in one of these formats along with the manuscript.

### D. Sizing of Graphics

Most charts, graphs, and tables are one column wide (3.5 inches/88 millimeters/21 picas) or page wide (7.16 inches/181 millimeters/43 picas). The maximum depth a graphic can be is 8.5 inches (216 millimeters/54 picas). When choosing the depth of a graphic, please allow space for a caption. Figures can be sized between column and page widths if the author chooses, however it is recommended that figures are not sized less than column width unless when necessary.

There is currently one publication with column measurements that do not coincide with those listed above. Proceedings of the IEEE has a column measurement of 3.25 inches (82.5 millimeters/19.5 picas).

The final printed size of author photographs is exactly 1 inch wide by 1.25 inches tall (25.4 millimeters  $\times$  31.75 millimeters/6 picas  $\times$  7.5 picas). Author photos printed in editorials measure 1.59 inches wide by 2 inches tall (40 millimeters  $\times$  50 millimeters/9.5 picas  $\times$  12 picas).

### E. Resolution

The proper resolution of your figures will depend on the type of figure it is as defined in the “Types of Figures” section. Author photographs, color, and grayscale figures should be at least 300dpi. Line art, including tables should be a minimum of 600dpi.

### F. Vector Art

In order to preserve the figures’ integrity across multiple computer platforms, we accept files in the following formats: .EPS/.PDF/.PS. All fonts must be embedded or text converted to outlines in order to achieve the best-quality results.

### G. Color Space

The term color space refers to the entire sum of colors that can be represented within the said medium. For our purposes, the three main color spaces are Grayscale, RGB (red/green/blue) and CMYK (cyan/magenta/yellow/black). RGB is generally used with on-screen graphics, whereas CMYK is used for printing purposes.

All color figures should be generated in RGB or CMYK color space. Grayscale images should be submitted in Grayscale color space. Line art may be provided in grayscale OR bitmap colorspace. Note that “bitmap colorspace” and “bitmap file format” are not the same thing. When bitmap color space is selected, .TIF/.TIFF/.PNG are the recommended file formats.

### H. Accepted Fonts Within Figures

When preparing your graphics IEEE suggests that you use of one of the following Open Type fonts: Times New Roman, Helvetica, Arial, Cambria, and Symbol. If you are supplying EPS, PS, or PDF files all fonts must be embedded. Some fonts may only be native to your operating system; without the fonts embedded, parts of the graphic may be distorted or missing.

A safe option when finalizing your figures is to strip out the fonts before you save the files, creating “outline” type. This converts fonts to artwork what will appear uniformly on any screen.

### I. Using Labels Within Figures

1) *Figure Axis labels* : Figure axis labels are often a source of confusion. Use words rather than symbols. As an example, write the quantity “Magnetization,” or “Magnetization M,” not just “M.” Put units in parentheses. Do not label axes only with units. As in Fig. 1, for example, write “Magnetization (A/m)” or “Magnetization (A·m<sup>-1</sup>),” not just “A/m.” Do not label axes with a ratio of quantities and units. For example, write “Temperature (K),” not “Temperature/K.”

Multipliers can be especially confusing. Write “Magnetization (kA/m)” or “Magnetization (10<sup>3</sup> A/m).” Do not write “Magnetization (A/m) × 1000” because the reader would not know whether the top axis label in Fig. 1 meant 16000 A/m or 0.016 A/m. Figure labels should be legible, approximately 8 to 10 point type.

2) *Subfigure Labels in Multipart Figures and Tables*: Multipart figures should be combined and labeled before final submission. Labels should appear centered below each subfigure in 8 point Times New Roman font in the format of (a) (b) (c).

### J. File Naming

Figures (line artwork or photographs) should be named starting with the first 5 letters of the author’s last name. The next characters in the filename should be the number that represents the sequential location of this image in your article. For example, in author “Anderson’s” paper, the first three figures would be named ander1.tif, ander2.tif, and ander3.ps.

Tables should contain only the body of the table (not the caption) and should be named similarly to figures, except that ‘.t’ is inserted in-between the author’s name and the table number. For example, author Anderson’s first three tables would be named ander.t1.tif, ander.t2.ps, ander.t3.eps.

Author photographs should be named using the first five characters of the pictured author’s last name. For example, four author photographs for a paper may be named: oppen.ps, moshc.tif, chen.eps, and duran.pdf.

If two authors or more have the same last name, their first initial(s) can be substituted for the fifth, fourth, third. . . letters of their surname until the degree where there is differentiation. For example, two authors Michael and Monica Oppenheimer’s photos would be named oppmi.tif, and oppmo.eps.

### K. Referencing a Figure or Table Within Your Paper

When referencing your figures and tables within your paper, use the abbreviation “Fig.” even at the beginning of a sentence. Do not abbreviate “Table.” Tables should be numbered with Roman Numerals.

### L. Submitting Your Graphics

Because IEEE will do the final formatting of your paper, you do not need to position figures and tables at the top and bottom of each column. In fact, all figures, figure captions, and tables can be placed at the end of your paper. In addition to, or even in lieu of submitting figures within your final manuscript, figures should be submitted individually, separate from the manuscript in one of the file formats listed above in Section IV-C. Place figure captions below the figures; place table titles above the tables. Please do not include captions as part of the figures, or put them in “text boxes” linked to the figures. Also, do not place borders around the outside of your figures.

### M. Color Processing/Printing in IEEE Journals

All IEEE Transactions, Journals, and Letters allow an author to publish color figures on IEEE Xplore® at no charge, and automatically convert them to grayscale for print versions. In most journals, figures and tables may alternatively be printed in color if an author chooses to do so. Please note that this service comes at an extra expense to the author. If you intend to have print color graphics, include a note with your final paper indicating which figures or tables you would like to be handled that way, and stating that you are willing to pay the additional fee.

## V. CONCLUSION

A conclusion section is not required. Although a conclusion may review the main points of the paper, do not replicate the abstract as the conclusion. A conclusion might elaborate on the importance of the work or suggest applications and extensions.

Appendixes, if needed, appear before the acknowledgment.

## ACKNOWLEDGMENT

The preferred spelling of the word “acknowledgment” in American English is without an “e” after the “g.” Use the singular heading even if you have many acknowledgments. Avoid expressions such as “One of us (S.B.A.) would like to thank . . . .” Instead, write “F. A. Author thanks . . . .” In most cases, sponsor and financial support acknowledgments are placed in the unnumbered footnote on the first page, not here.

## REFERENCES AND FOOTNOTES

### A. References

References need not be cited in text. When they are, they appear on the line, in square brackets, inside the punctuation. Multiple references are each numbered with separate brackets. When citing a section in a book, please give the relevant page numbers. In text, refer simply to the reference number. Do not use “Ref.” or “reference” except at the beginning of a sentence: “Reference [3] shows . . . .” Please do not use automatic endnotes in *Word*, rather, type the reference list at the end of the paper using the “References” style.

Reference numbers are set flush left and form a column of their own, hanging out beyond the body of the reference. The reference numbers are on the line, enclosed in square brackets. In all references, the given name of the author or editor is abbreviated to the initial only and precedes the last name. Use them all; use *et al.* only if names are not given. Use commas around Jr., Sr., and III in names. Abbreviate conference titles. When citing IEEE transactions, provide the issue number, page range, volume number, year, and/or month if available. When referencing a patent, provide the day and the month of issue, or application. References may not include all information; please obtain and include relevant information. Do not combine references. There must be only one reference with each number. If there is a URL included with the print reference, it can be included at the end of the reference.

Other than books, capitalize only the first word in a paper title, except for proper nouns and element symbols. For papers published in translation journals, please give the English citation first, followed by the original foreign-language citation. See the end of this document for formats and examples of common references. For a complete discussion of references and their formats, see the IEEE Editorial Style Manual for Authors at <https://journals.ieeeauthorcenter.ieee.org/wp-content/uploads/sites/7/IEEE-Editorial-Style-Manual-for-Authors.pdf>.

## B. Footnotes

Number footnotes separately in superscript numbers.<sup>1</sup> Place the actual footnote at the bottom of the column in which it is cited; do not put footnotes in the reference list (endnotes). Use letters for table footnotes (see Table I).

## APPENDIX I

### SUBMITTING YOUR PAPER FOR REVIEW

For more information about the submitting process, please see: <https://ieeexplore.ieee.org/Xplorehelp/author-center/submit-article-for-peer-review>. For inquiries regarding the submission of your paper, please contact [oprs-support@ieee.org](mailto:oprs-support@ieee.org).

## APPENDIX II

### IEEE PUBLISHING POLICY

The general IEEE policy requires that authors should only submit original work that has neither appeared elsewhere for publication, nor is under review for another refereed publication. The submitting author must disclose all prior publication(s) and current submissions when submitting a manuscript. Do not publish “preliminary” data or results. The submitting author is responsible for obtaining agreement of all coauthors and any consent required from employers or sponsors before submitting an article. The IEEE Transactions and Journals Department strongly discourages courtesy authorship; it is the obligation of the authors to cite only relevant prior work.

The IEEE Transactions and Journals Department does not publish conference records or proceedings, but can publish articles related to conferences that have undergone rigorous peer review.

## APPENDIX III

### PUBLICATION PRINCIPLES

The two types of contents of that are published are; 1) peer-reviewed and 2) archival. The Transactions and Journals Department publishes scholarly articles of archival value as well as tutorial expositions and critical reviews of classical subjects and topics of current interest.

Authors should consider the following points:

- 1) Technical papers submitted for publication must advance the state of knowledge and must cite relevant prior work.
- 2) The length of a submitted paper should be commensurate with the importance, or appropriate to the complexity, of the work. For example, an obvious extension of previously published work might not be appropriate for publication or might be adequately treated in just a few pages.
- 3) Authors must convince both peer reviewers and the editors of the scientific and technical merit of a paper; the standards of proof are higher when extraordinary or unexpected results are reported.
- 4) Because replication is required for scientific progress, papers submitted for publication must provide sufficient information to allow readers to perform similar

<sup>1</sup>It is recommended that footnotes be avoided (except for the unnumbered footnote with the receipt date on the first page). Instead, try to integrate the footnote information into the text.

experiments or calculations and use the reported results. Although not everything need be disclosed, a paper must contain new, useable, and fully described information. For example, a specimen's chemical composition need not be reported if the main purpose of a paper is to introduce a new measurement technique. Authors should expect to be challenged by reviewers if the results are not supported by adequate data and critical details.

- 5) Papers that describe ongoing work or announce the latest technical achievement, which are suitable for presentation at a professional conference, may not be appropriate for publication.

#### APPENDIX IV REFERENCE EXAMPLES

- *Basic format for books:*  
J. K. Author, "Title of chapter in the book," in *Title of His Published Book*, xth ed. City of Publisher, (only U.S. State), Country: Abbrev. of Publisher, year, ch. *x*, sec. *x*, pp. *xxx-xxx*.  
See [1], [2].
- *Basic format for periodicals:*  
J. K. Author, "Name of paper," *Abbrev. Title of Periodical*, vol. *x*, no. *x*, pp. *xxx-xxx*, Abbrev. Month, year, DOI: 10.1109.XXX.123456.  
See [3]– [5].
- *Basic format for reports:*  
J. K. Author, "Title of report," Abbrev. Name of Co., City of Co., Abbrev. State, Country, Rep. *xxx*, year.  
See [6], [7].
- *Basic format for handbooks:*  
*Name of Manual/Handbook*, *x* ed., Abbrev. Name of Co., City of Co., Abbrev. State, Country, year, pp. *xxx-xxx*.  
See [8], [9].
- *Basic format for books (when available online):*  
J. K. Author, "Title of chapter in the book," in *Title of Published Book*, *x*th ed. City of Publisher, State, Country: Abbrev. of Publisher, year, ch. *x*, sec. *x*, pp. *xxx-xxx*. [Online]. Available: <http://www.web.com>  
See [10]– [13].
- *Basic format for journals (when available online):*  
J. K. Author, "Name of paper," *Abbrev. Title of Periodical*, vol. *x*, no. *x*, pp. *xxx-xxx*, Abbrev. Month, year. Accessed on: Month, Day, year, DOI: 10.1109.XXX.123456, [Online].  
See [14]– [16].
- *Basic format for papers presented at conferences (when available online):*  
J.K. Author. (year, month). Title. presented at abbrev. conference title. [Type of Medium]. Available: site/path/file  
See [17].
- *Basic format for reports and handbooks (when available online):*  
J. K. Author. "Title of report," Company. City, State, Country. Rep. no., (optional: vol./issue), Date. [Online] Available: site/path/file  
See [18], [19].
- *Basic format for computer programs and electronic documents (when available online):*  
Legislative body. Number of Congress, Session. (year, month day). *Number of bill or resolution*, Title. [Type of medium]. Available: site/path/file  
**NOTE: ISO recommends that capitalization follow the accepted practice for the language or script in which the information is given.**  
See [20].
- *Basic format for patents (when available online):*  
Name of the invention, by inventor's name. (year, month day). Patent Number [Type of medium]. Available: site/path/file  
See [21].
- *Basic format for conference proceedings (published):*  
J. K. Author, "Title of paper," in *Abbreviated Name of Conf.*, City of Conf., Abbrev. State (if given), Country, year, pp. *xxxxxx*.  
See [22].
- *Example for papers presented at conferences (unpublished):*  
See [23].
- *Basic format for patents:*  
J. K. Author, "Title of patent," U.S. Patent *x xxx xxx*, Abbrev. Month, day, year.  
See [24].
- *Basic format for theses (M.S.) and dissertations (Ph.D.):*
  - 1) J. K. Author, "Title of thesis," M.S. thesis, Abbrev. Dept., Abbrev. Univ., City of Univ., Abbrev. State, year.
  - 2) J. K. Author, "Title of dissertation," Ph.D. dissertation, Abbrev. Dept., Abbrev. Univ., City of Univ., Abbrev. State, year.  
See [25], [26].
- *Basic format for the most common types of unpublished references:*
  - 1) J. K. Author, private communication, Abbrev. Month, year.
  - 2) J. K. Author, "Title of paper," unpublished.
  - 3) J. K. Author, "Title of paper," to be published.  
See [27]– [29].
- *Basic formats for standards:*
  - 1) *Title of Standard*, Standard number, date.
  - 2) *Title of Standard*, Standard number, Corporate author, location, date.  
See [30], [31].
- *Article number in reference examples:*  
See [32], [33].
- *Example when using et al.:*  
See [34].

#### REFERENCES

- [1] G. O. Young, "Synthetic structure of industrial plastics," in *Plastics*, 2<sup>nd</sup> ed., vol. 3, J. Peters, Ed. New York, NY, USA: McGraw-Hill, 1964, pp. 15–64.
- [2] W.-K. Chen, *Linear Networks and Systems*. Belmont, CA, USA: Wadsworth, 1993, pp. 123–135.

- [3] J. U. Duncombe, "Infrared navigation—Part I: An assessment of feasibility," *IEEE Trans. Electron Devices*, vol. ED-11, no. 1, pp. 34–39, Jan. 1959, 10.1109/TED.2016.2628402.
- [4] E. P. Wigner, "Theory of traveling-wave optical laser," *Phys. Rev.*, vol. 134, pp. A635–A646, Dec. 1965.
- [5] E. H. Miller, "A note on reflector arrays," *IEEE Trans. Antennas Propagat.*, to be published.
- [6] E. E. Reber, R. L. Michell, and C. J. Carter, "Oxygen absorption in the earth's atmosphere," Aerospace Corp., Los Angeles, CA, USA, Tech. Rep. TR-0200 (4230-46)-3, Nov. 1988.
- [7] J. H. Davis and J. R. Cogdell, "Calibration program for the 16-foot antenna," Elect. Eng. Res. Lab., Univ. Texas, Austin, TX, USA, Tech. Memo. NGL-006-69-3, Nov. 15, 1987.
- [8] *Transmission Systems for Communications*, 3<sup>rd</sup> ed., Western Electric Co., Winston-Salem, NC, USA, 1985, pp. 44–60.
- [9] *Motorola Semiconductor Data Manual*, Motorola Semiconductor Products Inc., Phoenix, AZ, USA, 1989.
- [10] G. O. Young, "Synthetic structure of industrial plastics," in *Plastics*, vol. 3, Polymers of Hexadromicon, J. Peters, Ed., 2<sup>nd</sup> ed. New York, NY, USA: McGraw-Hill, 1964, pp. 15-64. [Online]. Available: <http://www.bookref.com>.
- [11] *The Founders' Constitution*, Philip B. Kurland and Ralph Lerner, eds., Chicago, IL, USA: Univ. Chicago Press, 1987. [Online]. Available: <http://press-pubs.uchicago.edu/founders/>
- [12] *The Terahertz Wave eBook*. ZOmega Terahertz Corp., 2014. [Online]. Available: [http://dl.z-thz.com/eBook/zomega\\_ebook.pdf.1206\\_sr.pdf](http://dl.z-thz.com/eBook/zomega_ebook.pdf.1206_sr.pdf). Accessed on: May 19, 2014.
- [13] Philip B. Kurland and Ralph Lerner, eds., *The Founders' Constitution*. Chicago, IL, USA: Univ. of Chicago Press, 1987, Accessed on: Feb. 28, 2010, [Online] Available: <http://press-pubs.uchicago.edu/founders/>
- [14] J. S. Turner, "New directions in communications," *IEEE J. Sel. Areas Commun.*, vol. 13, no. 1, pp. 11–23, Jan. 1995.
- [15] W. P. Risk, G. S. Kino, and H. J. Shaw, "Fiber-optic frequency shifter using a surface acoustic wave incident at an oblique angle," *Opt. Lett.*, vol. 11, no. 2, pp. 115–117, Feb. 1986.
- [16] P. Kopyt *et al.*, "Electric properties of graphene-based conductive layers from DC up to terahertz range," *IEEE THz Sci. Technol.*, to be published. DOI: 10.1109/THZ.2016.2544142.
- [17] PROCESS Corporation, Boston, MA, USA. Intranets: Internet technologies deployed behind the firewall for corporate productivity. Presented at INET96 Annual Meeting. [Online]. Available: <http://home.process.com/Intranets/wp2.htm>
- [18] R. J. Hijmans and J. van Etten, "Raster: Geographic analysis and modeling with raster data," R Package Version 2.0-12, Jan. 12, 2012. [Online]. Available: <http://CRAN.R-project.org/package=raster>
- [19] Teralyzer. Lytera ÜG, Kirchhain, Germany [Online]. Available: [http://www.lytera.de/Terahertz\\_THz\\_Spectroscopy.php?id=home](http://www.lytera.de/Terahertz_THz_Spectroscopy.php?id=home), Accessed on: Jun. 5, 2014
- [20] U.S. House. 102<sup>nd</sup> Congress, 1<sup>st</sup> Session. (1991, Jan. 11). *H. Con. Res. 1, Sense of the Congress on Approval of Military Action*. [Online]. Available: LEXIS Library: GENFED File: BILLS
- [21] Musical toothbrush with mirror, by L.M.R. Brooks. (1992, May 19). Patent D 326 189 [Online]. Available: NEXIS Library: LEXPAT File: DES
- [22] D. B. Payne and J. R. Stern, "Wavelength-switched passively coupled single-mode optical network," in *Proc. IOOC-ECOC*, Boston, MA, USA, 1985, pp. 585–590.
- [23] D. Ebehard and E. Voges, "Digital single sideband detection for interferometric sensors," presented at the 2<sup>nd</sup> Int. Conf. Optical Fiber Sensors, Stuttgart, Germany, Jan. 2-5, 1984.
- [24] G. Brandli and M. Dick, "Alternating current fed power supply," U.S. Patent 4 084 217, Nov. 4, 1978.
- [25] J. O. Williams, "Narrow-band analyzer," Ph.D. dissertation, Dept. Elect. Eng., Harvard Univ., Cambridge, MA, USA, 1993.
- [26] N. Kawasaki, "Parametric study of thermal and chemical nonequilibrium nozzle flow," M.S. thesis, Dept. Electron. Eng., Osaka Univ., Osaka, Japan, 1993.
- [27] A. Harrison, private communication, May 1995.
- [28] B. Smith, "An approach to graphs of linear forms," unpublished.
- [29] A. Brahms, "Representation error for real numbers in binary computer arithmetic," IEEE Computer Group Repository, Paper R-67-85.
- [30] IEEE Criteria for Class IE Electric Systems, IEEE Standard 308, 1969.
- [31] Letter Symbols for Quantities, ANSI Standard Y10.5-1968.
- [32] R. Fardel, M. Nagel, F. Nuesch, T. Lippert, and A. Wokaun, "Fabrication of organic light emitting diode pixels by laser-assisted forward transfer," *Appl. Phys. Lett.*, vol. 91, no. 6, Aug. 2007, Art. no. 061103.
- [33] J. Zhang and N. Tansu, "Optical gain and laser characteristics of InGaN quantum wells on ternary InGaN substrates," *IEEE Photon. J.*, vol. 5, no. 2, Apr. 2013, Art. no. 2600111
- [34] S. Azodolmolky *et al.*, Experimental demonstration of an impairment aware network planning and operation tool for transparent/translucent optical networks," *J. Lightw. Technol.*, vol. 29, no. 4, pp. 439–448, Sep. 2011.



**First A. Author** (M'76–SM'81–F'87) and all authors may include biographies. Biographies are often not included in conference-related papers. This author became a Member (M) of IEEE in 1976, a Senior Member (SM) in 1981, and a Fellow (F) in 1987. The first paragraph may contain a place and/or date of birth (list place, then date). Next, the author's educational background is listed. The degrees should be listed with type of degree in what field, which institution, city, state, and country, and year the degree was earned. The author's major field of study should be lower-cased.

The second paragraph uses the pronoun of the person (he or she) and not the author's last name. It lists military and work experience, including summer and fellowship jobs. Job titles are capitalized. The current job must have a location; previous positions may be listed without one. Information concerning previous publications may be included. Try not to list more than three books or published articles. The format for listing publishers of a book within the biography is: title of book (publisher name, year) similar to a reference. Current and previous research interests end the paragraph. The third paragraph begins with the author's title and last name (e.g., Dr. Smith, Prof. Jones, Mr. Kajor, Ms. Hunter). List any memberships in professional societies other than the IEEE. Finally, list any awards and work for IEEE committees and publications. If a photograph is provided, it should be of good quality, and professional-looking. Following are two examples of an author's biography.



**Second B. Author** was born in Greenwich Village, New York, NY, USA in 1977. He received the B.S. and M.S. degrees in aerospace engineering from the University of Virginia, Charlottesville, in 2001 and the Ph.D. degree in mechanical engineering from Drexel University, Philadelphia, PA, in 2008.

From 2001 to 2004, he was a Research Assistant with the Princeton Plasma Physics Laboratory. Since 2009, he has been an Assistant Professor with the Mechanical Engineering Department, Texas A&M University, College Station. He is the author of three books, more than 150 articles, and more than 70 inventions. His research interests include high-pressure and high-density nonthermal plasma discharge processes and applications, microscale plasma discharges, discharges in liquids, spectroscopic diagnostics, plasma propulsion, and innovation plasma applications. He is an Associate Editor of the journal *Earth, Moon, Planets*, and holds two patents.

Dr. Author was a recipient of the International Association of Geomagnetism and Aeronomy Young Scientist Award for Excellence in 2008, and the IEEE Electromagnetic Compatibility Society Best Symposium Paper Award in 2011.



**Third C. Author, Jr.** (M'87) received the B.S. degree in mechanical engineering from National Chung Cheng University, Chiayi, Taiwan, in 2004 and the M.S. degree in mechanical engineering from National Tsing Hua University, Hsinchu, Taiwan, in 2006. He is currently pursuing the Ph.D. degree in mechanical engineering at Texas A&M University, College Station, TX, USA.

From 2008 to 2009, he was a Research Assistant with the Institute of Physics, Academia Sinica, Taipei, Taiwan. His research interest includes the development of surface processing and biological/medical treatment techniques using nonthermal atmospheric pressure plasmas, fundamental study of plasma sources, and fabrication of micro- or nanostructured surfaces.

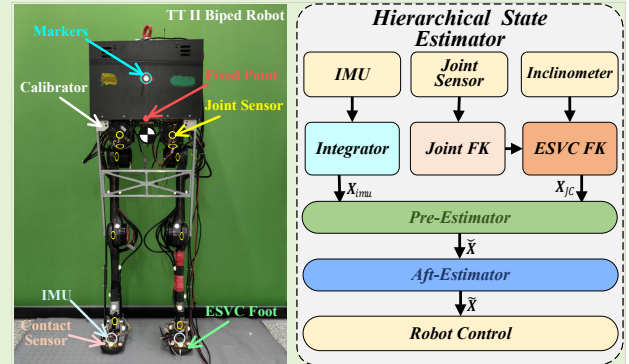
Mr. Author's awards and honors include the Frew Fellowship (Australian Academy of Science), the I. I. Rabi Prize (APS), the European Frequency and Time Forum Award, the Carl Zeiss Research Award, the William F. Meggers Award and the Adolph Lomb Medal (OSA).

# Noise Analysis and Hierarchical Adaptive Body State Estimator For Biped Robot Walking With ESVC Foot

Boyang Chen, Xizhe Zang, Chao Song, Yue Zhang, Xuehe Zhang and Jie Zhao

**Abstract**—The ESVC(Ellipse-based Segmental Varying Curvature) foot, a robot foot design inspired by the rollover shape of the human foot, significantly enhances the energy efficiency of the robot walking gait. However, due to the tilt of the supporting leg, the error of the contact model are amplified, making robot state estimation more challenging. Therefore, this paper focuses on the noise analysis and state estimation for robot walking with the ESVC foot. First, through physical robot experiments, we investigate the effect of the ESVC foot on robot measurement noise and process noise. and a noise-time regression model using sliding window strategy is developed. Then, a hierarchical adaptive state estimator for biped robots with the ESVC foot is proposed. The state estimator consists of two stages: pre-estimation and post-estimation. In the pre-estimation stage, a data fusion-based estimation is employed to process the sensory data. During post-estimation, the acceleration of center of mass is first estimated, and then the noise covariance matrices are adjusted based on the regression model. Following that, an EKF(Extended Kalman Filter) based approach is applied to estimate the centroid state during robot walking. Physical experiments demonstrate that the proposed adaptive state estimator for biped robot walking with the ESVC foot not only provides higher precision than both EKF and Adaptive EKF, but also converges faster under varying noise conditions.

**Index Terms**— Adaptive state estimation, biped locomotion, curvature foot, noise measurement.



## I. INTRODUCTION

**B**IPEDAL robot technology has made significant progress in recent years, such as G1 from Unitree [1], Atlas of Boston Dynamics [2] and Digit designed by Agility Robotics [3]. In laboratory environment, robots have already demonstrated impressive motion capabilities that are close to, or even surpass, those of humans. However, from the prospective of practical application, numerous challenges still exist, among which gait energy efficiency and ground adaptability are particularly important. When excluding upper limb operations, the foot, as the only part interacting with the external environment, directly affect the evolution of the entire robot system. Therefore, to improve bipedal walking performance, various foot designs for different scenarios have been investigated and implemented [4] [5] [6] [7].

This work was supported in part by the Major Research Plan of the National Natural Science Foundation of China (92048301).

Boyang Chen, Xizhe Zang, Chao Song, Yue Zhang, Xuehe Zhang and Jie Zhao are with the School of Mechatronics Engineering, Harbin Institute of Technology, Harbing 150001, China (e-mail: chenboyang@stu.hit.edu.cn, zangxizhe@hit.edu.cn, songchao@stu.hit.edu.cn, yzhanghit@stu.hit.edu.cn, zhangxuehe@hit.edu.cn, jzhao@hit.edu.cn).

Corresponding authors: Chao Song; Xuehe Zhang.

Among these studies, a key question is that how to effectively integrate foot design with robot locomotion and fully exploit the performance enhancements provided by the meticulous foot designs. This question is challenging and a prerequisite is that how the foot designs influence locomotion dynamics. In particular, the impact of the foot designs on walking-state variations needs careful consideration. In other words, from a feedback control perspective, understanding the effect of foot design on system noise and ensuring accurate state estimation are indispensable.

In terms of rollover shape, mainstream robot foot designs can be categorized as: arched foot [8], point foot [9], flat foot [10], line foot [11], arc/curved foot [6] [12], bionic foot [13] and flexible heterogeneous foot [14]. Among them, point foot, line foot, and flat foot are the most widely used. The point foot, with negligible mass, maintains point contact with the ground at all times in both the sagittal and coronal planes, greatly simplifying the modeling and control of biped robots, but it cannot provide sufficient frictional torque. The line foot maintains line contact in the sagittal plane and point contact in the coronal plane, compensating for the lack of friction of point foot. However, its energy efficiency is much lower than that of arc/curved or bionic designs. Moreover, line foot

and point foot lack sufficient sensory equipment so the foot data and body state have to be estimated through additional methods. The flat foot can compensate for the shortcomings of both; however, maintaining full contact requires the supporting foot to remain parallel to the ground at all times. This necessitates actuation of the ankle joint in both the pitch and roll directions, which in turn hinders the mass centralization of the robot. Additionally, the impact energy dissipation caused by the contact also results in lower gait efficiency. The bionic foot and flexible heterogeneous foot are not discussed in this paper due to their complexity and specific application scenarios.

In fact, it is difficult to find a generalized principle for robot foot design currently, especially when balancing multiple design criteria. Therefore the rollover shape of human foot serves as a good bionic template. Researchers in prosthetics and human anatomy have found that the bionic rollover shape can be divided into three parts: the fore-foot, mid-foot, and hind-foot. Each segment exhibits a varying curvature, with the heel and toes being more curved, while the mid segment remains relatively flat. The segmented varying curvature configuration allows for higher energy efficiency during human biped walking [15] [16] [17]. Inspired by this an ellipse based segmental varying curvature foot (ESVC foot) has been proposed in our previous work [12]. Multiple elliptical arcs are engaged to approximate the configuration of the rollover shape of human foot. Physical experiments on TT II robot illustrate that the foot design significantly improves the gait energy efficiency, especially when there exists lateral velocity. During walking, the support leg of the robot with ESVC foot undergoes a passive rotation in coronal plane and the contact point will rollover along the elliptical arcs. As the analytical form of the contact model does not exist due to the incomplete elliptic integral, an approximation contact model based on elementary functions is provide in our previous research. However, despite the simplicity of this method, the modeling error cannot be eliminated, and the error is amplified by the support leg rotation during robot walking. This means that directly using joint state data to obtain the robot body state is too coarse and sensitive for feedback control. Hence, this paper we try to reveal how the ESVC foot affect noise distribution of the robot system and focuses on the state estimation with ESVC foot.

The state estimation of bipedal robot has long been a focus of researchers, as it serves as a crucial foundation for feedback control. Due to the high dimensional non-linearity of the legged robot system, the extended Kalman filter(EKF) based method is widely used for state estimation [18], [19], [20], [21], [22]. By setting the process noise and measurement noise covariance as constant, Chen et al. [19] used the EKF to estimate the state of a fixed point(FP). The center of mass(CoM) state is then approximated through the FP and incorporated into feedback control based on the linear inverted pendulum model. This method is suitable for slower robot walking, where the FP behaves similarly to the CoM. Kang et.al. [20] proposed a nonlinear distributed state estimation framework for legged robot system. Through EKF and moving horizon estimation, the linear and angular states of the robot floating base can be estimated decoupledly, while maintaining a balance between

accuracy and computational efficiency is feasible. Gao et al. [22] proposed a robust adaptive state estimator based on the Invariant Extended Kalman Filter(IEKF), and by segmenting the design of adaptive adjustment factors, the estimator can adjust the noise covariance dynamically, and in their physical experiments, the velocity estimation of CoM demonstrated around 50% improvement compared to the original IEKF. Kim et.al. [23] redefined the state estimation as a Maximum A Posteriori (MAP) problem, achieving estimation results comparable to the IEKF under different contact conditions. Youm et.al. [24] proposed a learning-based approach that combines the Neural Measurement Network with EKF, significantly reducing position drift. The network is trained using only simulation data.

This paper focuses on the impact of the ESVC foot to the system noise and state estimation of walking bipedal robots. The contributions are as follows: first, we investigate the impact of the ESVC foot and contact model error on the robot measurement noise and process noise through physical experiments. Then a temporal regression model for noise covariance is developed using sliding window strategy and weighted cubic regression. Finally, we propose a hierarchical adaptive state estimator based on the temporal model. Under feedback control using the Hybrid Linear Inverted Pendulum (HLIP) [25], the proposed state estimator not only accurately provides body state data during robot walking, but also converges rapidly when the walking gait varying, compared to the classical EKF and the adaptive variants with fixed noise covariance.

The organization of this paper is as follows: In Section II.a, we review the ESVC foot model and demonstrate how to obtain the sensory data of robot state through the approximation model. In Section II.b, we first reveal the distribution of measurement noise and process noise through fixed point trajectory tracking experiments and physical walking experiments, respectively. Then the temporal regression model is designed for the initial guess of estimation. In Section III, we discuss the hierarchical adaptive state estimator. Section IV presents the validation and evaluation of the proposed state estimator. Conclusions and future work are presented in Section V.

## II. NOISE ANALYSIS AND APPROXIMATION

### A. Sensory State Data Acquisition

The quality of sensory data directly impacts the body state estimation, especially when errors are introduced by the varying contact point model of the ESVC foot. In order to investigate the impact, we equipped the ESVC foot to bipedal robot TT II as shown in the abstract figure. To acquire the sensory body state data relative to the contact frame, including the center of mass and the swing foot, six virtual joints are typically introduced to describe the robot motion with respect to the inertial frame which allows the body state can be calculated in a manipulator-like manner. However, this method is susceptible to sensory noise and also increases the computational load on the onboard controller. In our previous work [12], we derived the spatial transformation matrices

of foot upper center frame, foot fixed frame and contact point frame. Through the ESVC kinematics, we divide the configuration space into the internal space and the external space and the robot body state can be computed efficiently and decoupledly within the two spaces. In the internal space, the robot can be regarded as being fixed to the ground at the upper center frame of the support foot, making the sensory body state data only dependent on the joint states:

$$\mathbf{X}^{O_i} = f(\mathbf{q}_i, \dot{\mathbf{q}}_i). \quad (1)$$

For simplicity, we use  $O_i$  and  $C$  to denote the upper center frame of the support foot and contact frame, respectively. Then, in the external space, the sensory body state from joint space data calculation  $\mathbf{X}_{JC} = [\mathbf{p}_{JC}^C, \mathbf{v}_{JC}^C]^T$  with respect to the inertial frame can be obtained through the matrix  ${}^C_{O_i}\mathbf{T}_E$  and its derivatives  ${}^C_{O_i}\dot{\mathbf{T}}_E$ , which represents the transformation between frame  $O_i$  and frame  $C$  of ESVC foot, as shown in Eq.2. Since the transformation matrix is based on elementary functions and the derivatives can be obtain directly through numerical differencing, the calculation of the external space is simplified to a single matrix multiplication:

$$[\mathbf{p}_{JC}^C, 1, \mathbf{v}_{JC}^C, 1]^T = \begin{bmatrix} {}^C_{O_i}\mathbf{T}_E & 0 \\ {}^C_{O_i}\dot{\mathbf{T}}_E & {}^C_{O_i}\mathbf{T}_E \end{bmatrix} [\mathbf{p}^{O_i}, 1, \mathbf{v}^{O_i}, 1]^T \quad (2)$$

TT II robot is equipped with three groups of IMU and inclinometers, as shown in the top-right subfigure of the abstract figure. As two sensor groups are mounted on the surface of the ESVC foot to directly provide the states of both the swing and support foot, the matrix  ${}^C_{O_i}\mathbf{T}_E$  and  ${}^C_{O_i}\dot{\mathbf{T}}_E$  in Eq.2 can be calculated accordingly. The third group is mounted at a fixed position(FP) which is close to the CoM when standing, to obtain approximate state data of the CoM  $\mathbf{X}_{imu} = [\mathbf{p}_{imu}, \mathbf{v}_{imu}]^T$ . In other words, the TT II robot has two separate sources of sensory body state data,  $\mathbf{X}_{JC}$  and  $\mathbf{X}_{imu}$ .

## B. Noise Distribution And Approximation

In general, measurement noise and process noise are assumed to follow a Gaussian distribution, and their covariance matrices are often set as constant in state estimation. However, due to the complexity of bipedal system, the process covariance matrix often varies over time. Moreover, when the robot is equipped with the ESVC foot, its model error also affects the noise distribution. Therefore, in this section, we analyze the noise characteristics and determine the distribution of the robot with the ESVC foot through two experiments.

1) *Analysis of Measurement Noise*: Measurement noise is composed of the multiple sensors noise. For the two separate sources of sensory body state data of TT II, we use  $\sigma_{imu}^2 = [\sigma_{posimu}^2, \sigma_{velimu}^2]$  and  $\sigma_{JC}^2 = [\sigma_{posJC}^2, \sigma_{velJC}^2]$  to denote the measurement variance. The target trajectory of FP is designed to follow a path resembling the Lemniscate of Bernoulli. In the joint space, the actuators are controlled to accurately track the target joint position trajectory generated by the ESVC inverse kinematics. Several marker points are placed to indicate the positions of various body links of the robot, and a depth camera is employed to capture the joint angles.

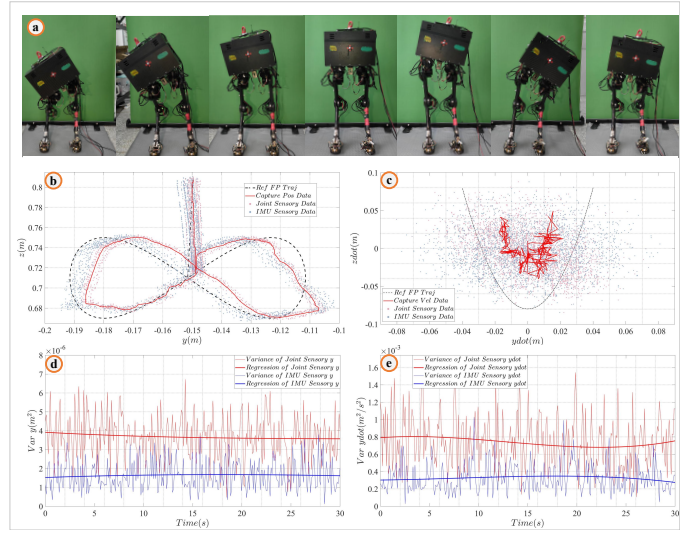


Fig. 1. (a). Snapshots FP trajectory tracking physical experiments on robot TT II. (b). Coronal FP position trajectory over ten experiments. (c). Coronal FP velocity trajectory over ten experiments. (d). FP position error variance distribution. (e). FP velocity error variance distribution.

To minimize the influence of mechanical clearances and motor backlash on measurement noise, the FP target trajectory is constrained to the coronal plane. As a result, the feet exhibit displacement only along the Y-axis and rotation about the X-axis. Although the foot roll angle is relatively small, its effect on the FP point cannot be neglected due to amplification caused by the supporting leg length. Finally, the position and velocity of the FP relative to the fixed frame are computed as ground truth using the URDF model, with two additional virtual joints introduced of the motion of Y-axis and X-axis.

Snapshots of the robot physical experiments are shown in Fig1.a. To eliminate random errors, the same experiment was repeated ten times, and the position and velocity of the FP in the coronal plane are depicted in Fig1.b and Fig1.c. The red points represent the sensory data from the configuration space, while the blue points indicate the data obtained from IMU integration. The dashed line denotes the reference trajectory and the solid lines show the ground truth obtained from the depth camera data. From the figure we find that the measurement noise exhibits characteristics of a Gaussian distribution. The variance vector  $\sigma^2$  of the two sensory body state data are computed using Eq.3.  $\mathbf{X}_{FPi}$  and  $\hat{\mathbf{X}}_{FPi}$  represent the ground truth and the measured state from sensory data of FP trajectory, respectively. Since the two sets of sensory state data are computed in the same manner, we use  $\sigma_{imu0}^2$  and  $\sigma_{JC0}^2$  to distinguish between them. We calculate the variance of measurement errors in position and velocity along the Y and Z directions at time intervals of 0.01 seconds, as shown in Fig1.d and Fig1.e. It can be observed from the figure that the measurement noise still remains nearly constant over time. Similar results can also be observed in the X direction. Therefore, the covariance matrices and of the two sensory state data of TT II robot can be approximated as constant diagonal matrices  $\sigma_{imu0}^2$  and  $\sigma_{JC0}^2$ , respectively, and their values can

be determined accordingly.

$$\sigma^2 = \frac{1}{n-1} \sum_{i=1}^n \left( \mathbf{X}_{FPi} - \hat{\mathbf{X}}_{FPi} \right)^2 \quad (3)$$

**2) Analysis of Process Noise:** Process noise is typically caused by mechanical clearances, motor backlash, and model inaccuracies. For bipedal robots with the ESVC foot, the elliptical arc length lacks a closed-form solution. To address this, our prior work introduced an approximation calculation based on elementary-function. However, the approximation errors in velocity and position are magnified by the leg length, thereby compromising the accuracy of body state estimation. Therefore, before designing the state estimator, it is essential to analyze the noise introduced by the ESVC foot and determine its distribution.

Open-loop marking time experiments on the TT II robot were conducted to investigate how modeling errors of the ESVC foot affect the system process noise. We first generate the desired CoM and swing foot target state trajectories using the HLIP model [25]. Since the ESVC foot operates in coronal plane, the approximate kinematic model is used to formulate contact point position constraints and friction cone constraints. These are incorporated into a full-order trajectory optimization based on DIRCON [27] to generate the desired joint trajectories. The orientation of swing foot is constrained to maintain parallel with the ground at all times. For HLIP model, the duration of single support phase is 0.42s and the orbit composition is SP1-CP2. The nominal step length during the left support phase(LSP) is  $-0.303\text{m}$ , which aligns with the relative positions of the left and right feet when the robot is in static standing posture. The target joint positions, velocities, and feedforward torques are obtained by solving the optimization and the robot is controlled to track the trajectories using PD feedforward control and gravity compensation. To ensure experimental repeatability, the TT II robot is initialized to a fixed posture by a calibration device, and then performs marking time by tracking the target joint trajectories, as depicted in Fig2.a. Of course, the robot inevitably tilts and falls over time. For analysis, we focus on several steps exhibiting relatively accurate tracking. The reference joint position and data are obtained by the depth camera while the orientation and angular velocity of the support foot are directly measured by an inclinometer and gyroscope mounted at the center of the foot upper plane. The event of support phase transition is determined by the onboard timer. Then the CoM state w.r.t contact point frame is calculated through forward kinematics with URDF file and ESVC foot model(Eq.2). Sixteen identical experiments were conducted to collect sample data. For clarity, a sampling interval of 0.08 seconds was used. The Y-direction position and velocity of five steps with better performance are plotted in Fig2.b and Fig2.c, respectively, where the color variation of each point indicates the corresponding sampling time.

It can be observed that even with the ESVC foot, the Y-direction position and velocity of the CoM approximately follow a normal distribution with clearly time-dependent characteristics. Similar results can also be observed in the X and Z directions. Moreover, significant discrepancies exist between

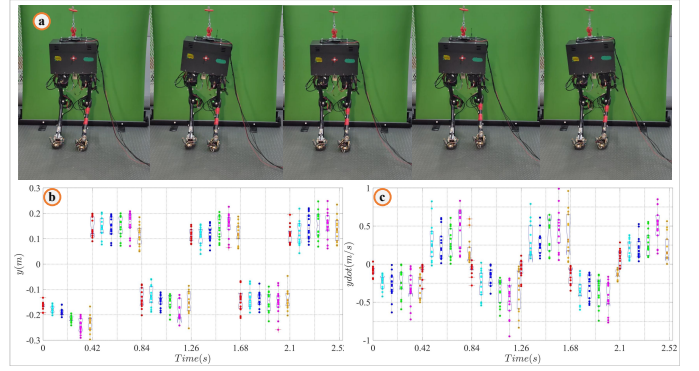


Fig. 2. (a) Snapshots of TT II marking time. (b) FP position trajectories over 16 experiments. (c) FP velocities trajectories over 16 experiments.

the experimental and theoretical trajectories in both velocity and direction, indicating that the TT II robot experiences relatively large process noise. Another noteworthy observation is that, for the Y-direction velocity, the measured data and the theoretical trajectory exhibit opposite signs at each step transition. For instance, the red points at the beginning of the third step in Fig2.c correspond to the transition from the RSP and LSP. Theoretically, the FP velocity in the Y direction should be positive at these transitions; however, the feedback data from the robot show a negative velocity, indicating that the swing foot made premature contact with the ground. Nevertheless, since the magnitude of the velocity is small, this indicates a premature contact of the swing foot.

**3) Regression of Process Noise:** To suppress the influence of incidental fluctuations, we first compute the average trajectory over the six selected steps. As the data storage frequency of robot system is 1kHz, each step for a single experiment will yield 420 data points. We divide the data points into 9 segments: the first eight segments each last 0.05s, and the final segment has a duration of 0.02s. Then the data from the six steps are subsequently merged into a single step, and the error variance trajectory of both CoM state is calculated accordingly. To analyze the error variance, the error variance trajectory is further divided into multiple sub-segments with each containing 20 knots and different weights are assigned to the variance points. Each sub-segment is referred to as a weighted variance window. The first eight segments are each associated with five weighted windows, whereas the final segment contains two. The variance at the center of each window is taken as the representative value of that window. By performing cubic polynomial regression to the representative values of these windows, the characteristics and variations of the process noise error variance within a single step can be clearly observed.

For a single weighted window, each variance point is assigned a weight based on its time offset from the segment endpoint, and the central value of the window is updated as

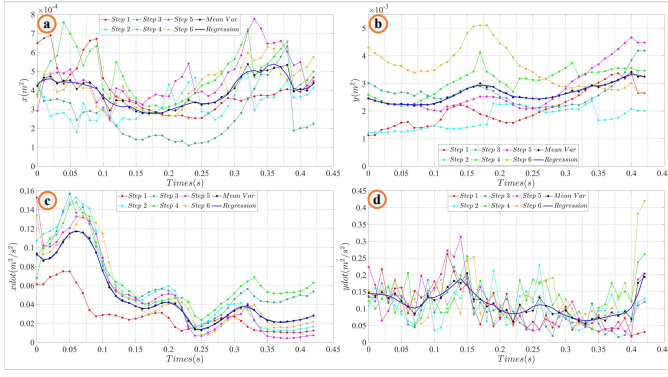


Fig. 3. Process error variance and regression results of TT II walking with ESVC foot over 16 experiments.

follows:

$$\begin{cases} \bar{y}_k = \frac{1}{N} \sum_{n=1}^N w_{k,n} y_{k,n} \\ w_{k,n} = e^{-\frac{(t_n - t_k)^2}{2\tau_w^2}} \end{cases} \quad (4)$$

$k$  is the index of current window.  $\bar{y}_k$  and  $y_{k,n}$  represent the representative value and the other data samples within the window, respectively.  $t_k$  and  $t_n$  are the corresponding time of  $\bar{y}_k$  and  $y_{k,n}$ .  $w_{k,n}$  is the weights of each point derived from Gaussian kernel function and  $\tau_w$  is smoothing parameter.

After processing the data, we used a regression model to extract temporal variation features. For the 9 data segments, the cubic polynomial regression is performed on window center value vector  $\bar{\mathbf{y}}_j$ . The resulted regression expression can be characterized as:

$$g_j = a_{j-1}t^3 + a_{j-2}t^2 + a_{j-3}t + a_{j-3} \quad (5)$$

$j$  is the index of the segment and  $g_j$  is the fitted value.  $t$  is the current sample time.  $\mathbf{a}_j = [a_{j-1}, a_{j-2}, a_{j-3}, a_{j-3}]^T$  represents the cubic parameters of current segment and can be calculated as:

$$\mathbf{a}_j = (\mathbf{t}_j^T \mathbf{t}_j)^{-1} \mathbf{t}_j^T \bar{\mathbf{y}}_j \quad (6)$$

$\mathbf{t}_j$  is the vector containing the sampling times of all window centers within this segment.

For different segments, a first-order continuity constraint is also enforced. Then the process error variances of the CoM position and velocity in both the X and Y directions are depicted in Fig3. The black curves denote the average variance of the selected steps and the blue curves represents the regression result. As shown in the figure, the process noise error variance in both the X and Y directions is strongly time-dependent, with trends that are smooth and easily fitted. This observation supports the development of state estimators and performance enhancement methods for robots employing the ESVC foot.

### III. HIERARCHICAL ADAPTIVE BODY STATE ESTIMATOR

In the previous section, we analyzed the impact of the ESVC foot on system noise of the TT II robot through physical FP tracking and marking time experiments. For the measurement

noise, it exhibited approximately constant error variance over time. For the process noise, we confirmed that despite the modeling errors introduced by the ESVC foot, it still approximately follows a normal distribution. This validates the use of a Gaussian model for characterizing the robot process noise, which is crucial for designing state estimators for bipedal robots with the ESVC foot. Based on these findings, this section presents the proposed adaptive state estimator.

The proposed body state estimator contains two layers. In the first layer, a pre-estimate of the robot sensory data is obtained based on fusion methods. For the second layer, an adaptive variation of extended Kalman filter(EKF) is employed to further update the CoM state with the temporal regression model.

#### A. Data Fusion Based Pre-Estimation

As described in secII, the TT II robot provides two types of direct sensory state,  $\mathbf{X}_{imu}$  and  $\mathbf{X}_{JC}$ . In this section, we use  $\check{\mathbf{X}}_i = [\check{\mathbf{p}}_i, \check{\mathbf{v}}_i]$  to represent the data at  $t_i$  after pre-estimation. Due to the significant differences between position and velocity errors, they are treated separately. For position, we directly fuse the two types of sensory position from the robot:

$$\check{\mathbf{p}}_i = \mathbf{p}_{JC.i} + \mathbf{K}_{pos}(\mathbf{p}_{imu.i} - \mathbf{p}_{JC.i}) \quad (7)$$

$\mathbf{K}_{pos}$  is a position fusion diagonal matrix composed of  $K_{posx}$ ,  $K_{posy}$  and  $K_{posz}$ . The optimal fusion parameter can be easily obtained by Eq.8:

$$\mathbf{K}_{pos.i} = \frac{\sigma_{JC.i}^2}{\sigma_{imu.i}^2 + \sigma_{JC.i}^2} \quad (8)$$

The error variance vector after fusing is  $\check{\sigma}_{prepos} = [\check{\sigma}_{prex}, \check{\sigma}_{prey}, \check{\sigma}_{prez}]^T$ . Since the two sensory data of the robot are decoupled, the parameters of position fusion are:

$$\check{\sigma}_{prepos}^2 = \begin{bmatrix} (1 - K_{posx})^2 & K_{posx}^2 \\ (1 - K_{posy})^2 & K_{posy}^2 \\ (1 - K_{posz})^2 & K_{posz}^2 \end{bmatrix} [\sigma_{JCpos}^2 \quad \sigma_{imupos}^2]^T \quad (9)$$

For velocity, since experimental observations indicate that joint velocity encoder errors increase significantly under vibrations, a two-step data fusion strategy is adopted. First, we construct a differential velocity  $\mathbf{v}_{diff.i}$  through  $\check{\mathbf{p}}$ :

$$\mathbf{v}_{diff.i} = \frac{\check{\mathbf{p}}_i - \check{\mathbf{p}}_{i-1}}{\sigma t} \quad (10)$$

$\sigma t$  is the sampling interval and the variance of  $\mathbf{v}_{diff.i}$  can be compute as:

$$\check{\sigma}_{diff}^2 = \begin{bmatrix} (1 - K_{posx})^2 & K_{posx}^2 \\ (1 - K_{posy})^2 & K_{posy}^2 \\ (1 - K_{posz})^2 & K_{posz}^2 \end{bmatrix} \begin{bmatrix} \sigma_{posJC}^2 & \sigma_{posimu}^2 \end{bmatrix}^T \quad (11)$$

At first step, we fuse  $\mathbf{v}_{diff.i}$  and  $\mathbf{v}_{imu.i}$  as shown in Eq.12. The corresponding fusion diagonal matrix  $\check{\mathbf{K}}_{vel}$  and error variance  $\check{\sigma}_{vel}^2$  is calculated analogously to  $\mathbf{K}_{pos}$  and  $\check{\sigma}_{pos}^2$ ,

as illustrated in Eq.12 and Eq.13.

$$\begin{cases} \bar{\mathbf{v}}_i = \mathbf{v}_{diff,i} + \bar{\mathbf{K}}_{vel}(\mathbf{v}_{imu,i} - \mathbf{v}_{diff,i}) \\ \bar{\mathbf{K}}_{vel} = \frac{\sigma_{diff}^2}{\sigma_{diff}^2 + \sigma_{velimu}^2} \end{cases} \quad (12)$$

$$\bar{\sigma}_{vel}^2 = \begin{bmatrix} (1 - K_{velx})^2 & K_{velx}^2 \\ (1 - K_{vely})^2 & K_{vely}^2 \\ (1 - K_{velz})^2 & K_{velz}^2 \end{bmatrix} [\sigma_{diff}^2 \quad \sigma_{velimu}^2]^T \quad (13)$$

At second step, the  $\bar{\mathbf{v}}_i$  is fused with joint sensory data  $\mathbf{v}_{JC,i}$  as described in Eq.14.  $\check{\mathbf{v}}_{ci}$  denotes the resulting velocity and  $\check{\mathbf{K}}_{vel}$  represents the fusion matrix. The error variance after second fusion  $\check{\sigma}_{vel}^2$  is depend on  $\bar{\sigma}_{vel}^2$  and  $\sigma_{velJC}^2$ , as shown in Eq.15.

$$\begin{cases} \check{\mathbf{v}}_i = \bar{\mathbf{v}}_{JC,i} + \check{\mathbf{K}}_{vel}(\bar{\mathbf{v}}_i - \mathbf{v}_{JC,i}) \\ \check{\mathbf{K}}_{vel} = \frac{\sigma_{JC,i}^2}{\sigma_{JC,i}^2 + \bar{\sigma}_{vel}^2} \end{cases} \quad (14)$$

$$\check{\sigma}_{vel}^2 = \begin{bmatrix} (1 - K_{velx})^2 & K_{velx}^2 \\ (1 - K_{vely})^2 & K_{vely}^2 \\ (1 - K_{velz})^2 & K_{velz}^2 \end{bmatrix} [\bar{\sigma}_{vel}^2 \quad \sigma_{velJC}^2]^T \quad (15)$$

### B. Adaptive post-Estimation

For the post-Estimation, the CoM state in X direction is denoted as  $\mathbf{X}_{comx,i} = [p_{x,i}, v_{x,i}]^T$  and its state transition equation and observation equation can be written as:

$$\begin{cases} \mathbf{X}_{comx,i+1} = \begin{bmatrix} 1 & \sigma t & \sigma t^2 \\ 0 & 1 & \sigma t \end{bmatrix} [\mathbf{X}_{comx,i} \quad \check{\mathbf{a}}_{x,i} + \boldsymbol{\omega}_i]^T \\ \mathbf{Z}_{comx,i+1} = \mathbf{H}_x [\check{p}_{comx,i} \quad \check{v}_{comx,i} + \phi_i]^T \end{cases} \quad (16)$$

$\check{\mathbf{a}}_{x,i}$  is the X direction component of the CoM acceleration  $\check{\mathbf{a}}_i$ .  $\mathbf{H}_x$  is the observation matrix and  $\mathbf{Z}_{comx,i+1}$  is the measurement state.  $\boldsymbol{\omega}_i$  and  $\phi_i$  represent the process noise and measurement noise, respectively. Before we perform EKF to Eq.16, the acceleration of CoM,  $\check{\mathbf{a}}_{x,i}$  should be determined. Although it is feasible to compute the CoM acceleration directly from foot contact forces and joint accelerations, modeling inaccuracies introduce errors in the results which will be infeasible for integration. Moreover, for the robot without contact force sensor, such as TT II and Cassie, the contact force need additional estimation that also increase the computational burden on the onboard system. It is worth noting that, since the robot is constrained to follow the HLIP model during walking, its CoM acceleration should closely match that of the HLIP behaviour. From another point, as an IMU is located at FP is close to the CoM, the sensor data can also be used to approximate the CoM acceleration. Then the acceleration of CoM can be obtained by fusing the acceleration of HLIP model and FP point:

$$\check{\mathbf{a}}_i = \mathbf{a}_{fp,i} + \mathbf{K}_a(\mathbf{a}_{hlip} - \mathbf{a}_{fp,i}) \quad (17)$$

$\mathbf{a}_{hlip} = \left[ \frac{\check{p}_{xi}}{h_0}, \frac{\check{p}_{yi}}{h_0}, 0 \right]^T$  is the theoretical acceleration of HLIP.  $\check{p}_{xi}$  and  $\check{p}_{yi}$  are the CoM position w.r.t. contact position.  $h_0$  is the target CoM height.  $\mathbf{K}_a$  is the fusion diagonal matrix composed of  $K_{ax,i}$ ,  $K_{ay,i}$  and  $K_{az,i}$ . As the CoM state approaches the theoretical model state, the HLIP acceleration

becomes more reliable, i.e.,  $\mathbf{K}_a$  tends toward 0. Conversely, when the CoM state deviates further from the model state, we place greater trust in the acceleration measured at the FP point. Therefore, a Gaussian kernel function is chosen to determine  $K_{ax,i}$ . Taking the X-direction as an example:

$$K_{ax,i} = e^{-\frac{(\bar{p}_{x,i} - p_{hx,i})^2 + (\bar{v}_{x,i} - v_{hx,i})^2}{2\tau_a^2}} \quad (18)$$

$p_{hx,i}$  and  $v_{hx,i}$  is the desired CoM state of HLIP,  $\tau_a$  is the smoothing parameter. At this point, both the state transition equation and observation equation in Eq.16 are fully defined.

As discussed in SecII, both measurement noise and process noise are approximately follow a Gaussian distribution and the error covariance matrices can be predicted at any time through the temporal regression model. It is important to note that the regression model is established based on the FP trajectory tracking task and the marking time task. In practice, when the robot changes its behavior, such as variations in walking speed or CoM height, the characteristics of both measurement noise and process noise should also change. Consequently, the error covariance matrices also need to be updated in time. In other words, it is impractical to analyze the noise characteristics for all possible robot motions and the post-estimation is required to adaptively update the covariance matrices. For bipedal robots, squatting and walking serve as templates for more complex motions. Therefore, the regression model derived from noise analysis can serve as an initial estimate for updating the current covariance matrices, and the subsequent updates will rollover with the historical covariance matrices. The measurement noise covariance and process noise covariance are updated as:

$$\begin{cases} \tilde{\mathbf{R}}_{C,i} = \alpha \mathbf{R}_{C,i} + (\mathbf{I} - \alpha) \hat{\mathbf{R}}_{C,i} \\ \tilde{\mathbf{Q}}_{C,i} = \beta_0 \mathbf{Q}_{C,i} + \beta_1 \hat{\mathbf{Q}}_{C,i} + \beta_2 \tilde{\mathbf{Q}}_{C,i-1} \end{cases} \quad (19)$$

$\tilde{\mathbf{R}}_{C,i}$  and  $\tilde{\mathbf{Q}}_{C,i}$  are the updated error covariance matrices of measurement noise and process noise, respectively, while  $\mathbf{R}_{C,i}$  and  $\mathbf{Q}_{C,i}$  represent the initial estimate covariance matrices which are initialized by  $\mathbf{R}_{C,0}$  and  $\mathbf{Q}_{C,0}$  from SecII.  $\hat{\mathbf{R}}_{C,i}$  and  $\hat{\mathbf{Q}}_{C,i}$  are estimated from the variance of residuals. For simplicity, we directly use the squared residuals. For the temporal characteristics of the process noise, the covariance matrix from the previous time step is used as the third term in the update loop.  $\alpha \in \mathbb{R}^{6 \times 6}$  is a constant measurement update parameter matrix, corresponding to the three-dimensional position and velocity of the CoM,  $\beta_0$ ,  $\beta_1$  and  $\beta_2$  are the process update parameter matrix which denotes the weights of initial estimate covariance matrices, measurement residuals and historical covariance matrix, respectively. And these matrices satisfy the constraint  $\beta_0 + \beta_1 + \beta_2 = \mathbf{I}_6$ . At this point, standard EKF operations can be applied to Eq.16, which are not elaborated here. Then the error variance  $\sigma_{JC,i}^2$  and  $\sigma_{imu,i}^2$  of sensory data still need to be updated, as shown in Eq.20.  $e_{JC,i}$  denotes the difference between CoM state  $\mathbf{X}_{JC,i}$  derived from joint sensory data and the post-estimated state  $\check{\mathbf{X}}_i$  and the update of  $\sigma_{imu,i}^2$  follows the same procedure as that of  $\sigma_{JC,i}^2$ . At the beginning of robot motion,  $\sigma_{imu,i}^2$  and

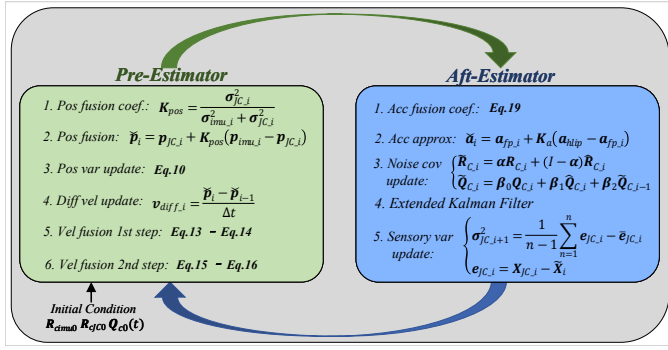


Fig. 4. The overall architecture of the proposed hierarchical body state estimator.

$\sigma_{JC_i}^2$  are initialized using  $\sigma_{imu0}^2$  and  $\sigma_{JC0}^2$ , respectively.

$$\begin{cases} \sigma_{JC,i+1}^2 = \frac{1}{n-1} \sum_{n=1}^N e_{JC,i}^2 - \bar{e}_{JC,i} \\ e_{JC,i} = X_{JC,i} - \tilde{X}_i \end{cases} \quad (20)$$

For clarity, the proposed hierarchical body state estimator is illustrated in Fig4. Components with a green background represent the data fusion-based pre-estimation stage, while those with a blue background correspond to the adaptive post-estimation.

## IV. EXPERIMENT EVALUATION

### A. Experimental Setup

To evaluate the proposed body state estimator, two types of physical experiments were conducted on the TT II robot: marking time and variable-speed lateral walking. The joints of TT II are actuated by AK-8064, a high-power motor designed by Cubemars [28]. The onboard computer is an Intel i7-8665U processor running Xenomai 3.2 real-time Linux as the main controller. The robot communication network is based on CAN network and all the sensory data are returned by HWT-9073-CAN developed by WIT MOTION [29]. Each ESVC foot is equipped with four pressure sensors for contact detection. The robot is controlled to follow the HLIP model, with the swing foot trajectory generated using cubic Hermite spline. The target joint space trajectory is synthesized through optimization-based phased inverse kinematics(PIK) and solved by the DRAKE robotics toolbox [30]. The actuated joints track the reference trajectory via PD control with feedforward compensation.

### B. Marking Time

To verify the accuracy of the estimator, marking time experiment was conducted on the TT II robot and the snapshots of a complete step is shown in Fig5.a. Acquiring the true states of a dynamic system is inherently challenging and an approximate ground truth is established by capturing joint kinematic data with a depth camera and reflective markers. Then the CoM trajectory using forward kinematics derived from the URDF model. The CoM phase portrait of Y-direction and Z-direction are shown in Fig5.b and Fig5.c, respectively.

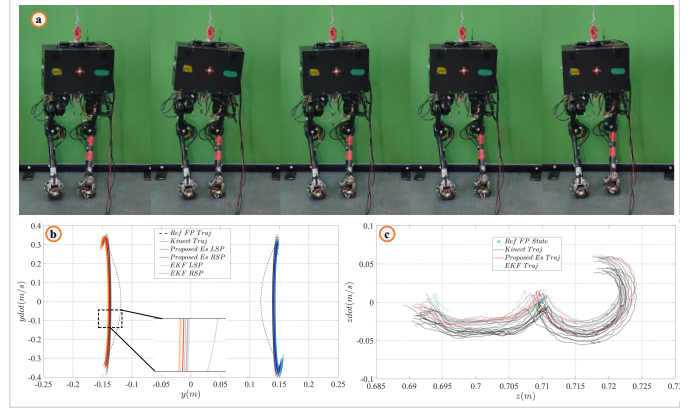


Fig. 5. (a). The snapshots of marking time experiment with TT II; (b). CoM phase portrait of Y-direction; (c). CoM phase portrait in Z-direction.

The black dashed line represents the reference trajectory of the HLIP model, while the dark gray solid line denotes the ground truth of the walking center of mass. The red and blue curves represent the feedback data estimated by the proposed method, corresponding to the left support phase and the right support phase. From the figure, it can be observed that the CoM states estimated by the proposed method closely approximate the ground truth during marking time. However, due to inherent measurement errors, the vision-based feedback also deviates to some extent from the true values. To provide a comparative baseline, we also introduce the EKF, as indicated by the orange and sky blue curves in Fig5.b and Fig5.c. Through comparison, it is observed that the proposed estimator can stably provide accurate state estimates during robot locomotion, with slightly better performance than the EKF-based method.

### C. Variable-speed Lateral Walking

To evaluate the performance of the state estimator under more complex locomotion conditions, a variable-speed lateral walking experiment was conducted. The TT II robot was controlled to decelerate from lateral walking at 0.1m/s to marking time, and then accelerate to a lateral walking speed of 0.2m/s, as illustrated in Fig6. Given the increased difficulty in obtaining accurate ground truth during dynamic walking, the EKF-based estimation is adopted as the reference baseline for comparison in this section. To further evaluate the adaptability of the proposed state estimator, the Adaptive EKF(AEKF) is also included as a baseline for comparison. The number of steps required for the robot to reach stable walking is used as the evaluation criterion. To highlight the influence of the ESVC foot, the variation of the CoM position in the Y-direction over time is plotted in Fig6. The red and blue curves represent the state estimates obtained by the proposed method during the LSP and RSP phases, respectively. The EKF results are shown in orange and sky blue, while the Adaptive EKF (AEKF) estimates are depicted in brown and navy blue. Through observation, we find that during steady walking, all three estimators exhibit comparable accuracy, and their outputs are sufficient to enable stable walking of the robot equipped with the ESVC foot. In the acceleration and deceleration phases, the convergence performance of the three

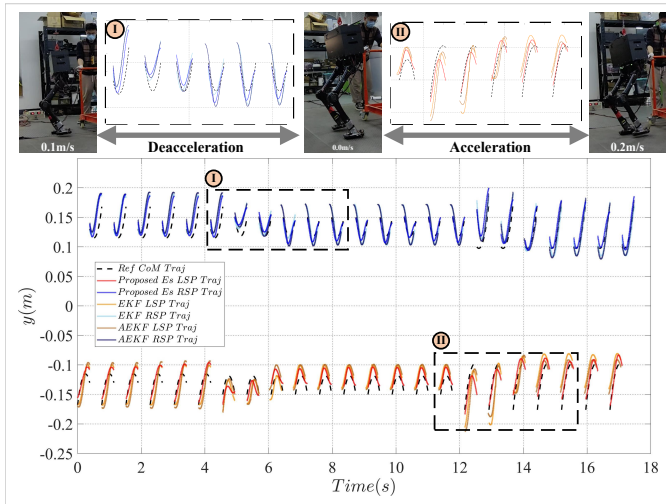


Fig. 6. Performance evaluation of EKF, AEKF and proposed estimator through CoM position in Y-direction.

estimators varies significantly. The trajectories corresponding to the acceleration and deceleration phases are magnified and presented in the upper section of Fig6. In the deceleration phase, the HLIP theoretical model plans the transition within two steps. In contrast, the robot employing the proposed estimator completed the deceleration over four steps, primarily due to modeling inaccuracies and residual estimation errors relative to the true states. The AEKF-based method also completed the deceleration during the fourth LSP, whereas the EKF required until the sixth RSP step to complete the transition. This indicates that both the proposed state estimator and the AEKF exhibit faster convergence than the EKF. In the acceleration phase, the robot using the proposed estimator reached the target stable state also within four steps, while both the AEKF and EKF required six steps to achieve stability. This demonstrates that the proposed estimator achieves faster convergence and, consequently, exhibits better adaptability compared to both EKF and AEKF.

## V. CONCLUSION

This paper investigates body state estimation for bipedal robots equipped with an ESVC (Ellipse-based Segmental Varying Curvature) foot—a bioinspired design that improves gait efficiency but introduces modeling uncertainties due to complex foot–ground interactions. Physical experiments are conducted to determine the distribution of measurement and process noise, and a time-varying fitting model of covariance matrix is constructed via weighted cubic polynomial regression. A hierarchical adaptive estimator is proposed, consisting of a multi-sensor data fusion–based pre-estimation stage and an adaptive post-estimation stage. In physical marking-time and variable-speed lateral walking, the proposed state estimation method delivers performance comparable to that of the AEKF and slightly better than the EKF. Moreover, when the robot’s motion changes, the proposed estimator demonstrates superior adaptability compared to both EKF and AEKF.

## REFERENCES

- [1] G1 Biped Robot. Available: <https://www.unitree.com/cn/g1>.
- [2] Atlas Biped Robot. Available: <https://bostondynamics.com/atlas>.
- [3] Digit Biped Robot. Available: <https://www.agilityrobotics.com/solution>.
- [4] R. H. Crompton, W. Sellers, K. Davids, J. McClymont, "Biomechanics and the origins of human bipedal walking: The last 50 years." *Journal of biomechanics*, vol. 157, p. 111701, 2023.
- [5] I. Frizza, K. Ayusawa, A. Cherubini, H. Kaminaga, P. Fraisse, and G. Venture, "Humanoids' feet: State-of-the-art & future directions," *International Journal of Humanoid Robotics*, vol. 19, no. 1, Mar. 2022, Art. no. 2250001.
- [6] A. Smyrli, M. Ghiassi, A. Kecskeméthy, and E. Papadopoulos, "On the effect of semielliptical foot shape on the energetic efficiency of passive bipedal gait," *IEEE/RSJ International Conference on Intelligent Robots and Systems (IROS)*, Macau, China, pp. 6302–6307, Nov. 2019.
- [7] A. Smyrli and E. Papadopoulos, "Modeling, Validation, and Design Investigation of a Passive Biped Walker with Knees and Biomimetic Feet," *2022 International Conference on Robotics and Automation (ICRA)*, Philadelphia, PA, USA, pp. 193–199, 2022.
- [8] J. Li, Y. Tian, X. Huang, and L. Wang, "Foot shape for passive dynamic kneed biped robot," *IEEE International Conference on Robotics and Biomimetics (ROBIO)*, pp. 1281–1286, Dec. 2010.
- [9] L. Han, X. Chen, Z. Yu, X. Zhu, K. Hashimoto, and Q. Huang, "Trajectory-free dynamic locomotion using key trend states for biped robots with point feet," *Science China Information Sciences*, vol. 66, Aug. 2023, Art. no. 189201.
- [10] Z. Liu, J. Gao, X. Rao, S. Ding, and D. Liu, "Complex dynamics of the passive biped robot with flat feet: Gait bifurcation, intermittency and crisis," *Mechanism and Machine Theory*, vol. 191, Jan. 2024, Art. no. 105500. Available: <http://www.bookref.com>.
- [11] G. García, R. Griffin, and J. Pratt, "MPC-based locomotion control of bipedal robots with line-feet contact using centroidal dynamics," *Humanoids*, Munich, Germany, pp. 1–8, Jul. 2021.
- [12] Boyang Chen and Xizhe Zang and Chao Song and Yue Zhang and Jie Zhao, "Model Analysis And Design Of Ellipse Based Segmented Varying Curved Foot For Biped Robot Walking", [arXiv:2506.07283](https://arxiv.org/abs/2506.07283), <https://arxiv.org/abs/2506.07283>, cs.RO, 2025.
- [13] B. Li, G. Xu, Z. Teng, et al., "Intelligent ankle–foot prosthesis based on human structure and motion bionics," *Journal of NeuroEngineering and Rehabilitation*, vol. 21, no. 1, Jan. 2024, Art. no. 119.
- [14] C. Piazza, C. Della Santina, G. M. Gasparri, and A. Bicchi, "Toward an adaptive foot for natural walking," in *Proceedings of the 2016 IEEE-RAS 16th International Conference on Humanoid Robots (Humanoids)*, Cancun, Mexico, pp. 1204–1210, Nov. 2016.
- [15] L. Ren, D. Howard, L. Ren, C. Nester, and L. Tian, "A generic analytical foot rollover model for predicting translational ankle kinematics in gait simulation studies," *Journal of Biomechanics*, vol. 43, no. 2, pp. 194–202, Jan. 2010.
- [16] P. Mahmoodi, R. S. Ransing, and M. I. Friswell, "Modelling the effect of 'heel to toe' roll-over contact on the walking dynamics of passive biped robots," *Applied Mathematical Modelling*, vol. 37, no. 12–13, pp. 7352–7373, Jun. 2013.
- [17] Q. Mei, H. K. Kim, L. Xiang, V. Shim, A. Wang, J. S. Baker, Y. Gu, and J. Fernandez, "Toward improved understanding of foot shape, foot posture, and foot biomechanics during running: A narrative review," *Frontiers in Physiology*, vol. 13, pp. 1–12, Dec. 2022, Art. no. 1062598.
- [18] T. Mikołajczyk, E. Mikołajewska, H. F. N. Al-Shuka, T. Malinowski, A. Kłodowski, D. Y. Pimenov, T. Paczkowski, F. Hu, K. Giasin, D. Mikołajewski, and M. Macko, "Recent advances in bipedal walking robots: Review of gait, drive, sensors and control systems," *Sensors*, vol. 22, no. 12, pp. 1–31, Jun. 2022, Art. no. 4440.
- [19] C.-P. Chen, J.-Y. Chen, C.-K. Huang, J.-C. Lu, and P.-C. Lin, "Sensor data fusion for body state estimation in a bipedal robot and its feedback control application for stable walking," *Sensors*, vol. 15, no. 3, pp. 4925–4946, Feb. 2015.
- [20] J. Kang, Y. Wang, and X. Xiong, "Fast decentralized state estimation for legged robot locomotion via EKF and MHE," *IEEE Robotics and Automation Letters*, vol. 9, no. 12, pp. 1–8, Dec. 2024, Art. no. 3483043.
- [21] T.-Y. Lin, R. Zhang, J. Yu, and M. Ghaffari, "Legged robot state estimation using invariant Kalman filtering and learned contact events," *arXiv preprint arXiv:2106.15713*, Jun. 2021.
- [22] C. Gao, Y. Xie, S. Zhu, and Y. Wang, "Adaptive robust invariant extended Kalman filtering for biped robot," in *Proceedings of the 2022 IEEE International Conference on Robotics and Biomimetics (ROBIO)*, Xishuangbanna, China, pp. 1885–1891, Dec. 2022.

- [23] H. Kim, S. Hong, G. Ji, S. Jeon, J. Hwangbo, J.-H. Oh, and H.-W. Park, "Legged robot state estimation with dynamic contact event information," *IEEE Robotics and Automation Letters*, vol. 6, no. 4, pp. 6733–6740, Oct. 2021.
- [24] D. Youm, H. Oh, S. Choi, H. Kim, and J. Hwangbo, "Legged robot state estimation with invariant extended Kalman filter using neural measurement network," arXiv preprint arXiv:2402.00366, Feb. 2024.
- [25] X. Xiong, A. Ames, "3-d underactuated bipedal walking via h-hip based gait synthesis and stepping stabilization". *IEEE Transactions on Robotics*, vol. 38, no. 4, pp. 2405-2425, Aug. 2022.
- [26] Suppliment Data, Available: <https://github.com/cby-gh/Estimation-ESVC-FOOT>
- [27] B. Chen, X. Zang, Y. Zhang, L. Gao, Y. Zhu, and J. Zhao, "A non-flat terrain biped gait planner based on DIRCON," *Biomimetics*, vol. 7, no. 4, pp. 1–18, Nov. 2022, Art. no. 203.
- [28] Joint Actuator, Available: <https://www.cubemars.com/cn/goods-1143-AK80-64.html>.
- [29] IMU & Inclinator, Available: <https://www.wit-motion.com/>.
- [30] Drake, Available: <https://drake.mit.edu/>.